Applications of One-dimensional Nanostructures in Energy Conversion and Biomedical Sciences

by

Eunice Mercado Feliciano

A dissertation submitted in partial fulfillment of the requirements for the degree of

DOCTOR OF PHILOSOPHY
in
APPLIED CHEMISTRY

UNIVERSITY OF PUERTO RICO
MAYAGÜEZ CAMPUS
2011

Approved by:

Miguel E. Castro, PhD President, Graduate Committee	Date
René S. Vieta Rivera, PhD Member, Graduate Committee	Date
Arturo J. Hernández Maldonado, PhD Member, Graduate Committee	Date
José A. Colucci Ríos, PhD Member, Graduate Committee	Date
Carlos Marín, PhD Representative of Graduate Studies	Date
Francis Patrón Chairperson of the Department	Date

Applications of One-dimensional Nanostructures in Energy Conversion and Biomedical Sciences

by: Eunice Mercado
Submitted to the Department of Chemistry
on December 5, 2011, in partial fulfillment of the
requirements for the degree of
Doctor of Philosophy

Abstract

This research explores applications of carbon nanotubes in energy and biomedical sciences. For applications in energy, this research reports the synthesis and characterization of one-dimensional silver nanostructures using single-wall carbon nanotubes (SWCNT) as a template material. Transmission electron microscopy (TEM) and scanning tunneling microscopy (STM) results are consistent with the formation of a one-dimensional array of silver particles on SWCNT. The correlation of the UV/Vis spectral results with those derived from the TEM and STM images analysis provides further insights into the silver nanostructures optical properties and morphology. There is evidence for the excitation of the longitudinal silver plasmon mode in the optical absorption spectra of the Ag-SWCNT dispersions, even at the lowest silver concentrations. The obtained results indicate that silver deposits on SWCNT have the potential to be light-to-energy conversion devices through the coupling of the electric field excited in arrays of plasmonic particles. In order to explore the nanotubes properties for the biomedical sciences field, single-wall and multi-wall carbon nanotubes were functionalized with amino groups. The functionalization makes possible the study of the tubes' interaction with the myoglobin protein in aqueous solution. The UV/Vis data obtained suggests that there are protein-nanotubes interactions.

Thesis Supervisor: Miguel E. Castro

Aplicaciones de Nanoestructuras Unidimensionales en Conversión de Energía y Ciencias Biomédicas

por: Eunice Mercado
Sometida al Departamento de Química
el 5 de diciembre de 2011, en cumplimiento parcial de los
requerimientos para el grado de
Doctor en Filosofía

Resumen

Este trabajo investiga aplicaciones de nanotubos de carbono en energía y ciencias biomédicas. En aplicaciones de energía, se reporta la síntesis y caracterización de nanoestructuras unidimensionales de plata utilizando nanotubos de carbono de pared simple (SWCNT) como material de templado. Resultados de microscopía de transmisión electrónica (TEM) y de rastreo por tunelaje (STM) son consistentes con un arreglo unidimensional de partículas de plata sobre los nanotubos de carbono. La correlación de los resultados obtenidos con UV/Vis y las imágenes obtenidas con el análisis de TEM y STM proveen información sobre las propiedades ópticas y morfología de las nanoestructuras de plata. Se observa evidencia de la excitación del modo longitudinal del plasmón de plata en el espectro de absorción óptico de dispersiones de Ag-SWCNT, aún a las menores concentraciones de plata. Los resultados obtenidos indican que los depósitos de plata sobre los SWCNT tienen potencial de dispositivos para la conversión de luz a energía a través del acoplamiento del campo electromagnético excitado en arreglos de partículas plasmónicas. En ciencias biomédicas, nanotubos de carbono de pared simple y pared múltiple fueron funcionalizados con grupos amino. La funcionalización hace posible el estudio de la interacción de los tubos con la proteína mioglobina en solución acuosa. Los datos de UV/Vis obtenidos sugieren interacciones proteína-nanotubos.

Consejero de Tésis: Dr. Miguel E. Castro

Este trabajo es dedicado a mi esposo

Milton Ernesto Rivera-Ramos,

y a mis hijos

Adrián Ernesto Rivera Mercado
y
Alana Lucía Rivera Mercado

Gracias por servirme siempre de apoyo, no dejaré nunca de darle gracias a Dios por la familia tan maravillosa que me ha regalado.

Acknowledgements

I wish to acknowledge my advisor Dr. Miguel E. Castro, for his direction in my research. I want to express gratitude as well for the support that I received from Dr. Edu Suárez during the discussions regarding the biomedicine area.

During the development of my graduate studies many other persons collaborated directly and indirectly with my research. Without their support it would have been difficult for me to finish my work. I want to particularly thank my first lab partners and friends, Priscila Santiago, Lidiany González, Madelline León and Edmy Ferrer, who gave me all their cooperation during my PhD studies. Also I want to say thanks to Steven Santiago and Luis Baez, for their help with the STM experiments. I wish to acknowledge the help of Eldy Román during the protein-nanotubes related experiments and to Dr. Milton E. Rivera-Ramos Research Group in UPR-Ponce, for helping with the carbon nanotubes modification. In addition, I would like to show gratitude to my colleagues in UPR-Ponce for their support during my PhD studies.

I also wish to acknowledge the financial support from the Alfred P. Sloan Foundation and Puerto Rico Industrial Development Company, Pridco.

Contents

Appendix Section

List of Figures

List of Tables

Chapter 1

Applications of one-dimensional nanostructures in energy conversion and biomedical sciences

1.1 Introduction

Carbon nanotubes have potential applications in fields such as electronics, nanotechnology, optics, and materials science among others. Carbon nanotubes are allotropic forms related to graphite. Assuming that graphite sheets can be rolled into a cylinder and their edges joined, nanotubes are formed. There are different types of carbon nanotubes because the graphitic sheets can be rolled in different ways. A nanotube may consist of one tube of graphite, called a single-wall nanotube (SWCNT), or of a number of concentric tubes called multi-wall nanotubes (MWCNT). Typically carbon nanotubes have diameters of a few nanometers. The wider the diameter of the nanotube, the more it behaves like graphite. Generally SWCNT have smaller diameters than MWCNT. The fact that electrical properties of SWCNT are much better than MWCNT, and the fact that inner tubes of MWCNTs do not contribute significantly to some

mechanical properties, make SWCNT more attractive for certain applications [1]. The structure of the nanotube influences its properties; including electrical properties, thermal conductivity, density, and lattice structure [2]. Research in this area has been very active since the end of the last decade and the beginning of the new millennium. Applications of carbon nanotubes cover many fields, including hydrogen storage. The broader impact of cost effective and efficient functional nanostructures for hydrogen storage includes (i) the miniaturization of fuel cells systems, (ii) facilitation of high-energy materials transportation from where it can be distributed, (iii) the acceleration in the implementation of environmentally friendly energy alternatives in vehicles, and (iv) the reduction of space used in the storage of high energy materials, which would result in a reduction of the environmentally hazard-disposed materials typically employed for gas storage.

Among all the fields of application where these structures can be used, this work focuses specifically in the study of possible applications in energy conversion and biomedical sciences.

1.2 Objectives

This research is divided in three components, and each one is explained by a thesis objective.

UPRM Research

In the Chemistry Department of the University of Puerto Rico at Mayagüez (UPRM) the study of the deposition and characterization of silver nanoparticles on single wall carbon nanotubes was carried out using optical absorption spectroscopy and electron microscopy.

Internship in Ponce School of Medicine Research

As part of an internship in the Ponce School of Medicine the interaction of the myoglobin protein with functionalized carbon nanotubes was studied.

Educational Research

A contribution to undergraduate education related to the interaction of light with matter was made by means of a technological tool named *The Science Portal*. The description of this component is included in the first part of the appendix section.

1.3 Overview of the Thesis

The first part of the work described here is the use of SWCNT as template material for silver nanoparticles. There is evidence for energy transfer through the electromagnetic coupling of adjacent silver nanoparticles. The electronic and optical properties of naked SWCNT are extremely sensitive to atomic structure, with distinctive energy-level structures corresponding to both metallic and semiconducting species [3]. This structure is characterized by two integers (n,m) that can be related to its diameter and its chirality. The absorption and emission spectra of carbon nanotubes has been the subject of various studies. In general, light absorption in the UV-visible region is a response of the electronic properties of a material. Fine structure has been documented in isolated carbon nanotubes or dispersed SWCNT in a solution [4, 5]. Electronic coupling among mixes energy states among the different SWCNT in a bundle, limit the observation of a fine structure. SWCNT electronic properties exhibit a strong structural dependence, which helps drive to promising applications. However, when the SWCNT are in bundled their efficient use is diminished [6]. The SWNTs used in this experiment consist of a 60 % semi metallic and 40% metallic structure. While we are not able to spot bands characteristic of individual SWCNT, the fine structure observed is consistent with the formation of SWCNT dispersions.

In recent years, efforts have also been devoted to exploring the potential biological applications of carbon nanotubes, motivated by their interesting size, shape, and structure, as well as attractive and unique physical properties [7]. With their small

diameters and lengths ranging from as short as 50 nm up to micrometers, SWCNTs are one-dimensional nanomaterials that can be used in biomedical research. The flexible one-dimensional nanotube may bend to facilitate multiple binding sites of a functionalized nanotube to one cell, and improved binding affinity of nanotubes conjugated with targeting ligands. With all atoms exposed on the surface, SWCNT have high surface area that allows efficient loading of multiple molecules along the length of the nanotube sidewall.

As a second part, this work explores the interaction between the myoglobin protein and surface modified SWCNT and MWCNT in aqueous solution, in order to contribute to the clinical detection of the protein associated with the rhabdomyolysis disease. This condition could be harmful to the kidney and frequently results in kidney damage. The UV/Vis measurements obtained suggest a protein-nanotubes interaction.

This research also includes an educational component that aims to strengthen students' knowledge in science and engineering concepts by developing a technological tool, named The Science Portal. As was stated before, the description of this part of the work is included in the appendix section. In this portal, students will use PC to PC connection technologies to access instrumentation not available in their campuses. The contribution make by the Science Portal is focused on the interaction of light with matter and the organization of atoms in matter.

1.4 References

1. Ha MLP, Grady BP, Lolli G, Resasco DE: Composites of Single-Walled Carbon Nanotubes and Styrene-Isoprene Copolymer Latices, Macromol. Chem. Phys. 2007, 208, 446–456.

2. Attal S, Thiruvengadathan R, Regev O: Determination of the concentration of single-walled carbon nanotubes in aqueous dispersions using UV-visible absorption spectroscopy, Anal Chem. 2006, 78(23):8098-104.

3. Sfeir MY, Beetz T, Wang F, Huang L, Huang XMH, Huang M, Hone J, O'Brien S, Misewich JA, Heinz TF, Wu L, Zhu Y, Brus LE: Optical Spectroscopy of Individual Single-Walled Carbon Nanotubes of Defined Chiral Structure, Science 2006, 312 (5773): 554 – 556.

4. Hartschuh A, Pedrosa HN, Peterson J, Huang L, Anger P, Qian H, Meixner AJ, Steiner M, Novotny L, Krauss TD: Single Carbon Nanotube Optical Spectroscopy, Chem. Phys. Chem 2005, 6, 1–6.

5. Weisman RB: Optical Spectroscopy of Single-Walled Carbon Nanotubes, Department of Chemistry, Center for Nanoscale Science and Technology, and Center for Biological and Environmental Nanotechnology, Rice University, Houston, Texas (To appear in: Contemporary Concepts of condensed matter Science, Volume 3 Elsevier)

6. Thess A, Lee R, Nikolaev P, Dai H, Petit P, Robert J, Xu C, Lee YH, Kim SG, Rinzler AG, Colbert DT, Scuseria GE, Tománek D, Fischer JE, Smalley RE: Crystalline Ropes of Metallic Carbon Nanotubes, Science, 1996, 273 (5274): 483 – 487.

7. Liu Z, Tabakman S, Welsher K, Dai H: Carbon Nanotubes in Biology and Medicine: In vitro and in vivo Detection, Imaging and Drug Delivery, Nano Res 2009 (2): 85-120.

Chapter 2

One-dimensional arrangement of silver nanoparticles for light to electrical energy conversion*

This chapter presents evidence for the justification of the use of single-wall carbon nanotubes as a template material for the one-dimensional arrangement of silver nanoparticles.

***** *Gonzalez L, Mercado E, Santiago P, Leon M, Morales M, Irizarry R, Castro ME: Functional Nanostructures by Wet Chemistry: A Tool to Ordered 1D and 3D Nanostructures, Nanoparticles: Synthesis, Stabilization, Passivation, and Functionalization, Chapter 7, 2008, pp 77-89.*

2.1 Introduction

Conversion of solar energy to forms that can be used in the different aspects of our lives has been a long standing question. Historically, solar energy to electrical energy conversion research has focused on the development of inorganic or organic materials with optical properties for optimum light absorption and the generation of carriers. These carriers are typically hot electrons-which may and may not be hole correlate. Electron scattering through collisions with other carriers or heavier nuclei are a significant factor limiting efficient solar energy to electrical energy conversion.

The scientific community has turned to the development of new concepts regarding solar energy to electrical energy conversion. The dielectric constant is a quantitative measure of the interaction of light with matter. When the dielectric constant (ε) is equal to zero (0), all the light is absorbed by the material and converted into a collective excitation of electrons. This collective of electrons oscillate at the plasma frequency (ω_p). Thus one photon absorption results in the excitation of many electrons as oppose to a single electronic excitation, where absorption of one photon results in the excitation of a single electron. There are two modes typically associated with this collective excitation: the transverse and the longitudinal modes.

Theoretical predictions and recent experimental evidence support the proposal that there is a strong coupling of the electric field associated with a plasma among adjacent nanoparticles allowing for energy transfer and communication among adjacent particles.

Efficient use of plasma excitation in solar to electrical energy conversion will ultimately require development of efficient methods for the preparation of one-dimensional arrays of nanoparticles.

This one-dimensional alignment may be identified by the excitation of the longitudinal plasmon mode in spherical particles. Isolated nanoparticles should exhibit only the excitation of the transverse plasmon mode. Figure 1 shows a representation of the excited plasmon modes that should be displayed by an isolated metallic nanoparticle, and a one-dimensional arrangement of the particles.

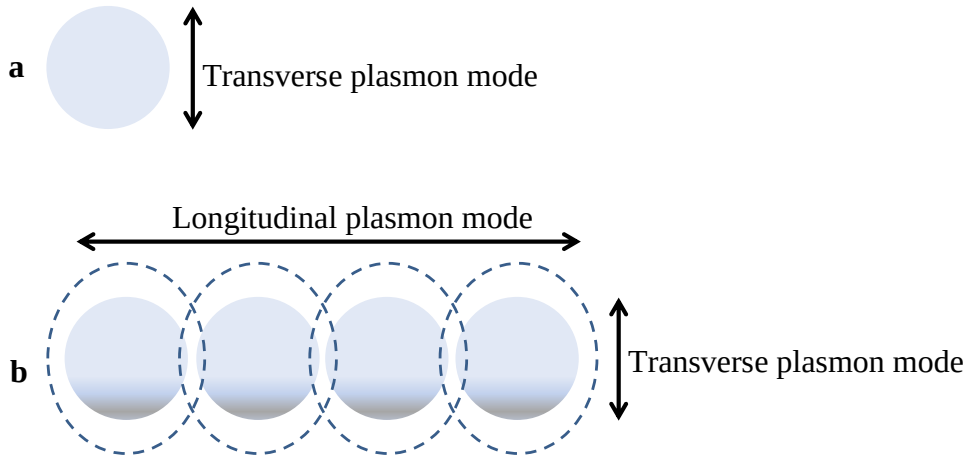

Figure 1: Excited plasmon modes excited in an isolated metallic nanoparticle, and in a one-dimensional arrangement of the particles. (a) Only the transverse plasmon mode is excited in an isolated metallic nanoparticle. (b) Coupling of the electric field among adjacent nanoparticles results in a longitudinal mode in a one-dimensional arrangement.

Previous work suggest that while an isolated metal nanoparticle constitutes a small plasmonic system, interactions within an ensemble of nanostructures can give rise to a much higher field confinement. Sweatlock et al. studied the coupling of linear arrays of silver nanoparticles in glass [1]. The coupling is attributed to the formation and interaction of the longitudinal plasmon mode in particles. Full-field simulations of the electromagnetic field distribution on arrays of closely spaced Ag nanoparticle arrays show that coupling between the plasmonic particle modes is enhanced by a short interparticle distance. By comparing the simulated data with the experimental optical absorption data they concluded that the observed plasmon coupling behavior is dominated by short arrays of touching particles and/or long arrays of strongly coupled particles. Pinchuk et al. found that a near-field coupling of the silver particles occurs when the interparticle distance is smaller than twice the particle diameter. This leads to pronounced red shifts in the plasmon resonance wavelength and increasing widths as the particle separation decreases [2]. Previous work with gold particles show a trend similar as the one observed with silver. Enoch et al. reported a broadening of the plasmon bandwidth of gold nanoparticles with a decrease of the interparticle distance [3]. This is interpreted in terms of the interaction between the surface charges formed at the particle surface and contributes to a pronounced difference between the absorption spectra of a single particle and a particle dimmer. They demonstrated that the electric near-field intensity maps around the dimers have completely different field distributions compared to the case of a single particle array. Maier et al. report the existence of longitudinal and transverse plasmon modes in chains of Au nanoparticles. The results support the validity

of an electromagnetic energy transfer below the diffraction limit along chains of closely spaced metal nanoparticles [4].

2.2 Results and discussion

Our research group had achieved the synthesis of one-dimensional silver nanostructures [5, 6]. This synthesis is based on wet chemistry. Figure 2 show a general approach employed to the synthesis of one-dimensional nanostructures.

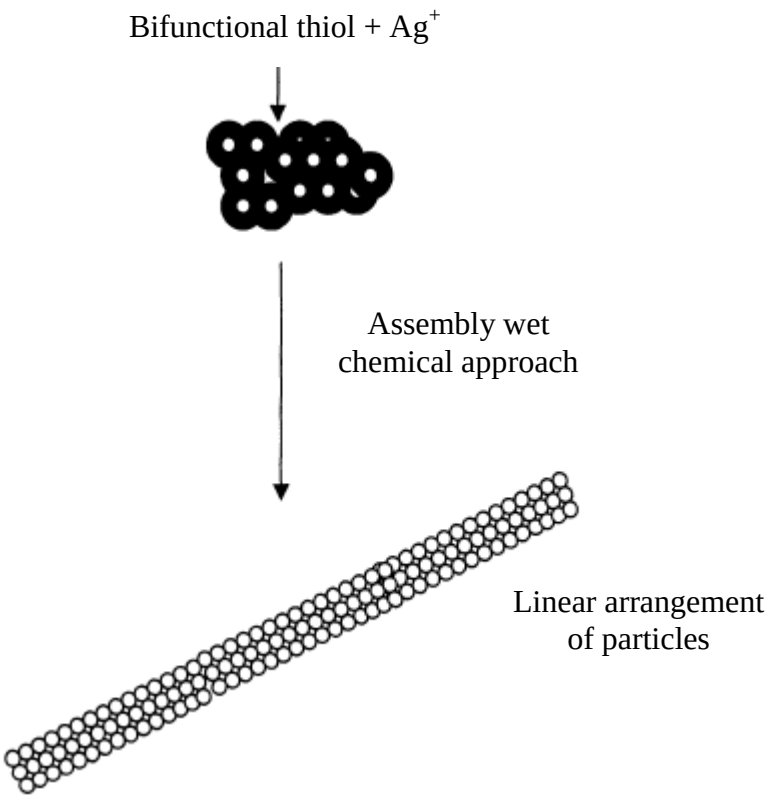

Figure 2: Representation of the concept of hydrogen bonding interactions among carboxylic acid end of alkyl thiols bonded to silver surfaces

One-dimensional silver nanostructures are developed by using a bifunctional thiol to couple two nanoparticles. In the case presented here, mercapto acetic acid ($HOOCCH_2SH$) was used as the chemical to drive the one dimensional assembly. The thiol adsorbs to the silver surface by the sulfur atom while the carboxylic acid group hydrogen bonds to adjacent carboxylic acid groups from a thiol adsorbed in a nearby particle. Since carboxylic acids can make only one hydrogen bonding interaction, a linear array of particles is formed. This linear array has been identified in dry deposits of $HOOCCH_2S$-Ag mixtures.

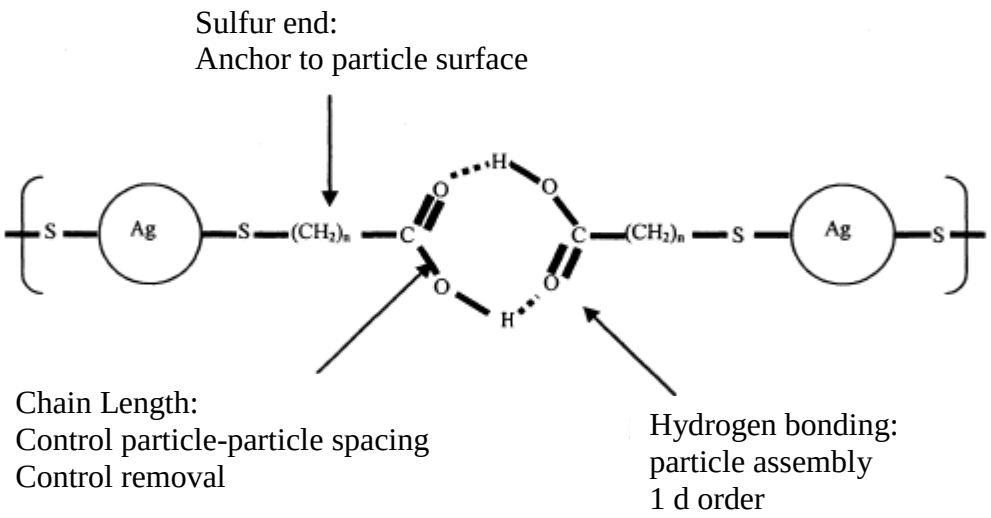

Figure 3: General approach employed to the synthesis of one-dimensional nanostructures. A thiol capped silver particle is assembled into one-dimensional nanostructure.

Representative electron microscopy measurements of micelles and dry deposits are displayed on figure 4 and 5, respectively. In solution, most of the $HOOCCH_2S$-Ag structures are solvated by water molecules, limiting the use of conventional optical

spectroscopy tools for their characterization. The one dimensional nanostructures are between 15 and 30 nm in diameter while their length varied from about 230 nm up to several micrometers.

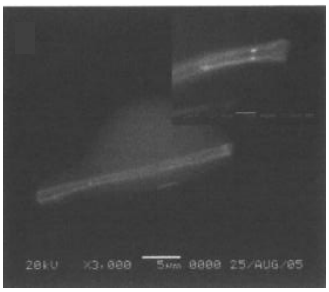

Figure 4: Wet SEM measurement of aqueous solution containing $HOOCCH_2S$-Ag.

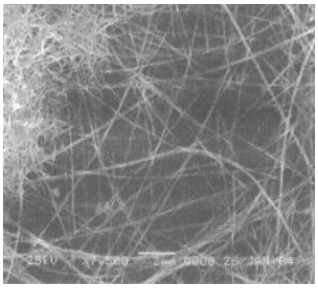

Figure 5: Scanning electron microscopy image of a dry deposit of a silver-thiol mixture diluted with 10.0 mL of water

The main problems found with this approach are that the one-dimensional nanostructures are formed in dry deposits limiting the use of optical microscopy tools to establish the excitation of the longitudinal plasmon mode and, mercapto acetic acid is a dangerous chemical. For that reason, we turned our focus on the use of carbon nanotubes to template one dimensional silver nanostructures.

2.3 References

1. Sweatlock LA, Maier SA, Atwater HA: Highly confined electromagnetic fields in arrays of strongly coupled Ag nanoparticles. Physical Review B, 2005, 71: 235408.

2. Pinchuk AO, Schatz GC: Nanoparticle optical properties: Far- and near-field electrodynamic coupling in a chain of silver spherical nanoparticles. Materials Science and Engineering B, 2008, 149: 251–258.

3. Enoch S, Quidant R, Badenes G: Optical sensing based on plasmon coupling in nanoparticle arrays. Optic Express, 2005, 12 (15):3422.

4. Maier SA, Brongersma ML, Kik PG, Atwater HA: Observation of near-field coupling in metal nanoparticle chains using far-field polarization spectroscopy. Physical Review B, 2002, 65, 193408.

5. Mercado E, Santiago S, Baez L, Rivera D, Gonzalez M, Rivera ME, Leon M, Castro ME, Nanoscale Research Letters 2011, 6:602.

6. Gonzalez L, Mercado E, Santiago P, Leon M, Morales M, Irizarry R, Castro ME: Functional Nanostructures by Wet Chemistry: A Tool to Ordered 1D and 3D Nanostructures, Nanoparticles: Synthesis, Stabilization, Passivation, and Functionalization, Chapter 7, 2008, pp 77-89.

Chapter 3

One-dimensional silver nanostructures on single-wall carbon nanotubes*

We report the synthesis and characterization of one-dimensional silver nanostructures using single-wall carbon nanotubes (SWCNT) as a template material. Transmission electron microscopy and scanning tunneling microscopy are consistent with the formation of a one-dimensional array of silver particles on SWCNT. We observed evidence for the excitation of the longitudinal silver plasmon mode in the optical absorption spectra of Ag-SWCNT dispersions, even in the lowest silver concentrations employed. The results indicate that silver deposits on SWCNT may be candidates for light-to-energy conversion through the coupling of the electric field excited in arrays of plasmonic particles.

* *Mercado E, Santiago S, Baez L, Rivera D, Gonzalez M, Rivera ME, Leon M, Castro ME, Nanoscale Research Letters 2011, 6:602.*

3.1 Introduction

There is a worldwide interest in the development of technologies for efficient use and conversion of sunlight into useful energy forms, including heat and electricity. Such technologies promise to result in economic benefits and improvement in the environment. Any rustic and simple energy conversion device must contain a material that absorbs light and converts it into an energy output. Several optical materials may have suitable properties for light absorption and energy conversion, but how to trap and conduct energy over a distance remains a fundamental question.

Electrons and holes have been the choice of charge transport in light-to-energy conversion [1, 2]. Electron scattering results in heating devices, but its applications are limited in the production of electrical energy. In recent years an innovative idea that has emerged, which takes advantage of the electric field generated by the excitation of plasmons in nanoparticles. The plasmon frequency corresponds to the energy at which the dielectric constant is zero, and all light is converted into the excitation of a group of electrons and the formation of an electric field. In isolated spherical nanoparticles, only the transverse plasmon mode is excited at the resonance frequency, while the longitudinal mode is readily observed in the optical absorption spectra of nanorods and nanowires [3, 4]. Theoretical predictions and recent experimental evidence support the proposal that there is a strong coupling among adjacent nanoparticles that enables the excitation of the longitudinal plasmon mode in particles aligned in one dimension [5, 6]. In practice, one-dimensional alignment of nanoparticles is not a simple task and requires a support. In this

regard, glass matrices and multiwall carbon nanotubes have been used to study coupling of the nanoparticles and their contribution to the longitudinal mode of the plasmon absorption band [7-11]. We report the use of single-wall carbon nanotubes (SWCNT) to template one-dimensional silver nanostructures.

Our findings are consistent with the deposition of silver nanoparticles on the SWCNT surface. As illustrated in Scheme 1, the reduction of the silver cations present in solution by the electron rich SWCNT results in the deposition of silver on the SWCNT surface. Further absorption of silver cations from the solution results in the formation of nanoparticles in close proximity to each other. Transmission electron microscopy (TEM) and scanning tunneling microscopy (STM) measurements of SWCNT with the lowest silver loads are consistent with the formation of discrete silver-rich regions on the nanotubes.

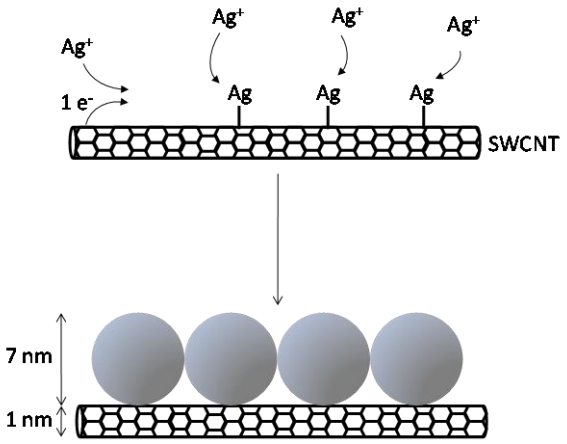

Scheme 1. Deposit of silver on SWCNT

We observe evidence for the optical excitation of the longitudinal silver plasmon mode, even with the lowest silver concentrations employed, a result consistent with simulations of light absorption by continuous one-dimensional nanostructures. The results encourage further research on the use of SWCNT as templates for the development of nanostructured plasmonic devices for the light to electrical energy conversion.

3.2 Experimental Section

3.2.1 Materials

The single-wall carbon nanotubes employed for the work described here were purchased from Cheap Tubes Inc (Brattleboro, VT, USA). The silver nitrate ($AgNO_3$) used in the silver nanoparticle synthesis and the ethylene glycol used as a solvent in our experiments were obtained from Sigma-Aldrich and used without further purification.

3.2.2 Equipment

UV-visible absorption measurements were conducted using an Agilent Spectrophotometer model 8453 (Biodirect, Inc., Taunton, MA, USA). A quartz cuvette with an optical path of 0.25 cm was used for the optical absorption measurements. Scanning tunneling microscopy (STM) measurements were performed in a NanoSurf Easy Scan E-STM **(**Nanosurf Inc., Boston, MA, USA**)**, version 2.1, using a Pt/Ir tip. The STM was calibrated with measurements performed on a commercial gold ruler. Measurements performed on longitudinal features of dry deposits of submonolayer quantities of C_{12}-SH and C_{10}-SH alkyl thiols coincided with the expected molecular

lengths of these molecules. A drop of the silver/SWCNT dispersion was deposited on a highly oriented graphite attached to a magnetic holder and allowed to dry prior to the measurements. TEM measurements were performed with a JEOL 2010 electron microscope (JEOL USA, Inc., Peabody, MA, USA). The samples were outgassed at 10^{-3} Torr for several days prior to placement in the TEM sample compartment. TEM measurements were performed with an acceleration voltage of 120 kV. Negatives of the micrographs were processed using standard techniques and scanned with an EPSON Perfection V750 PRO scanner (Epson, Long Beach, CA, USA) and stored in a PC computer for further analysis. Scanning electron microscopy measurements were performed with a JEOL 6460 LV SEM instrument (JEOL USA, Inc., Peabody, MA , USA) equipped with an X-ray detector for EDAX (Energy dispersive X-ray spectroscopy) measurements.

3.2.3 Silver nanoparticles synthesis

A 1×10^{-2} M $AgNO_3$ solution was prepared using ethylene glycol as solvent. Aliquots of the solution were used to prepare 5 ml of 1×10^{-3} and 1×10^{-5} M silver solutions. The amount of 0.0023 g of SWCNT was added to each solution which was then warmed to 470 K. The solutions were used to obtain the UV-visible measurements 24 h later. SEM and EDAX measurements were obtained from the solution with the highest silver concentration, 1×10^{-2} M. The formation of silver nanoparticles templated on SWCNT resulted from the solution with the lowest silver concentration, 1×10^{-5} M. A dry deposit of the solution was analyzed by TEM and STM techniques.

3.2.4 Computer Simulations

Simulations of the optical absorption spectra of silver spheres are based on Mie theory. The wavelength-dependent absorbance (A) of light by a substance is given by:

$$A = n\gamma I_o / \ln 10 \qquad (1)$$

where n represents the number of absorbers, γ is the extinction coefficient, and I_o is the incident light intensity. For spheres smaller than the wavelength of the incident light, the absorption cross section may be estimated by calculating the dipole contribution to the absorption spectra as:

$$\gamma = 9\varepsilon_\alpha^{3/2} V (\omega / c)\varepsilon_2 / \{[\varepsilon_1 + 2\varepsilon_2]^2 + \varepsilon_2^2\} \qquad (2)$$

where ε_α is the dielectric constant of the medium, ω is the frequency of the incoming radiation, c is the speed of light, and ε_1 and ε_2 represent the real and imaginary parts of the particle's dielectric constant (ε). In the case of silver, the real and imaginary parts of the dielectric constants have contributions from interband transitions (IB) and the excitation of the plasmon (P):

$$\varepsilon_1 = \varepsilon_{1IB} + \varepsilon_{1,P} \qquad \varepsilon_2 = \varepsilon_{2IB} + \varepsilon_{2P} \qquad (3)$$

The plasmon contributions to the components of the dielectric constant are calculated as:

$$\varepsilon_1 = 1 - \omega_P^2 / (\omega^2 + \omega_o^2) \qquad \varepsilon_2 = \omega_p^2 \omega_o / [\omega(\omega^2 + \omega_o^2)] \qquad (4)$$

where ω_P and ω represent the frequencies corresponding to the bulk plasmon and incident light, and ω_o is the size-dependent surface scattering rate estimated as:

$$\omega_o = A v_F / r \qquad (5)$$

where A is proportionality factor, v_F is the Fermi velocity, and r is the particle radii.

The simulations of the absorption spectra of the one-dimensional structures are based on the Gans treatment of Mie theory. The extinction coefficient within the dipole approximation is calculated as:

$$\frac{\gamma}{N_P V} = \frac{2\Pi \in_{\alpha}^{1/2}}{3\lambda} \sum_{j} \frac{\left(\frac{1}{P_j^{\,2}}\right) \in_2}{\left[\in_1 + \left(\frac{1-P_j}{P_j}\right) \in_{\alpha}\right]^2 + \in_2^2} \qquad (6)$$

where N_P and V represent particle concentration and volume, respectively, and λ is the incident light wavelength. The contributions of the real (ε_1) and imaginary (ε_2) components of the refractive index are obtained from Harris et al. [10]. In the equation, P_j represents a geometric factor related to the coordinates of an elliptical particle [12]. The letters used in the P_j represent the longitudinal axis "A" and transverse axes "B" and "C." In elongated ellipsoids, B and C are equal and represent the diameter (d) of the ellipsoid.

3.3 Results and Discussion

3.3.1 UV-visible absorption measurements

Figure 1 summarizes the absorption spectra of the SWCNT dispersions warmed in the presence of different $AgNO_3$ concentrations. For reference, the spectrum of a $AgNO_3$ solution in the absence of the SWCNT is also indicated. The optical absorption spectrum of the $AgNO_3$ solution does not exhibit any significant absorption features above 400 nm.

The absorption spectrum of the SWCNT dispersions employed for the experiments reported here are also indicated in the same figure.

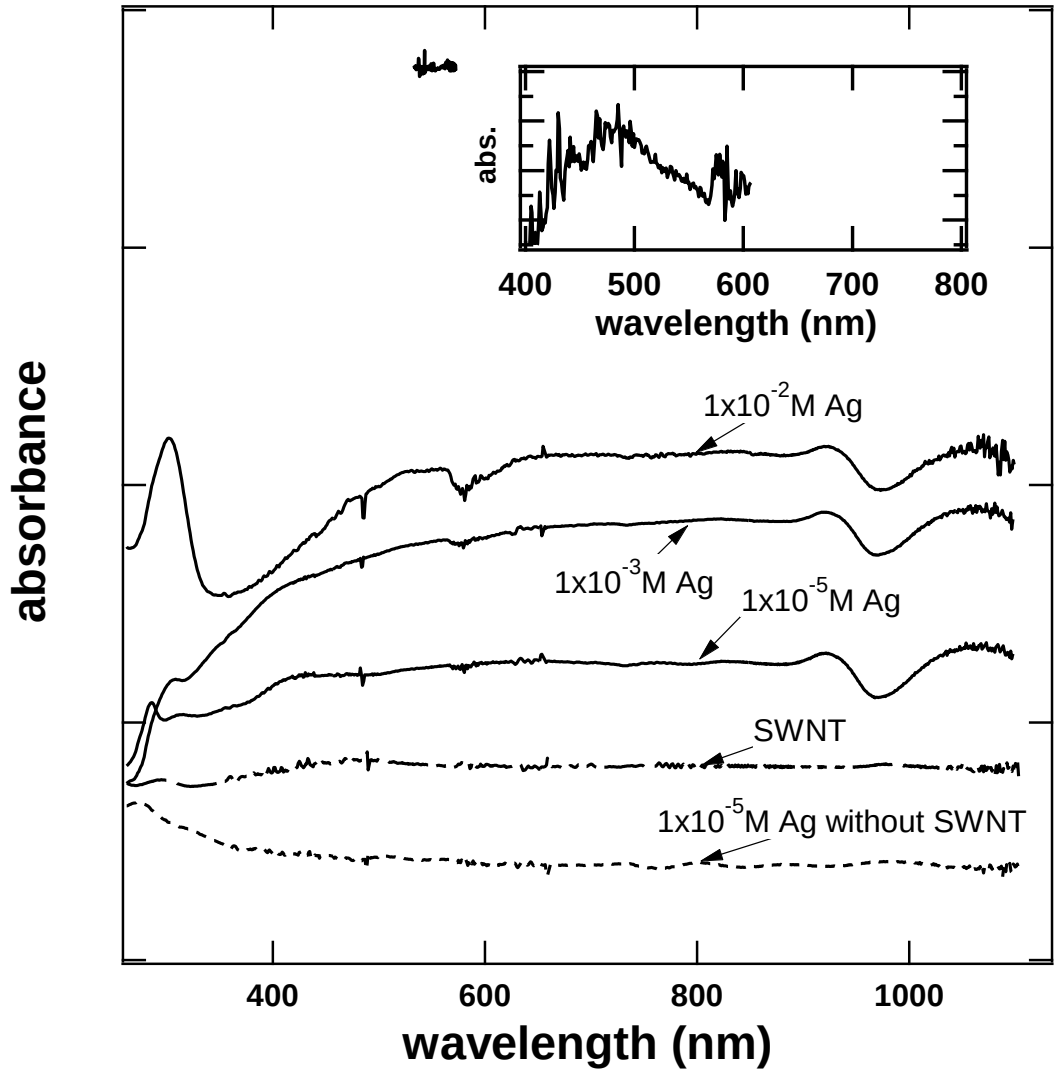

Figure 1. The UV-visible spectra of Ag-SWCNT dispersions. As a function of [$AgNO_3$] between 250 and 850 nm. Representative spectra of the SWCNT and [$AgNO_3$] solutions employed in the work are indicated in the figure.

The optical absorption spectrum of the SWCNT dispersion does not exhibit significant absorption above 400 nm, although considerable fine structure can be observed within the

noise level of the measurement. The insert in Figure 1 shows the optical absorption spectra for of the SWCNT dispersion between 400 and 800 nm multiplied by a factor of 60 to adjust it to the scale displayed with the other data. This fine structure is not noise as it is not observed in measurements of the solvent, cell, or air performed in the same instrument under otherwise identical experimental conditions. The absorption and emission spectra of carbon nanotubes have been the subject of various studies [13, 14]. Light absorption is a response of the electronic properties and structure of SWCNT corresponding to metallic, semi-metallic, and semiconducting structures. Fine structure has been documented in isolated carbon nanotubes or dispersions of SWCNT [15, 16]. When the carbon nanotubes are not dispersed, electronic coupling mixes energy states among different SWCNT in a bundle, limiting the observation of fine structure. The SWCNT used in this experiment consist of 60% semi-metallic and 40% metallic structures. While we are not able to spot bands characteristic of individual SWCNT, the fine structure observed is consistent with the formation of SWCNT dispersion in ethylene glycol.

The spectrum of the SWCNT dispersion is significantly affected by the presence of the $AgNO_3$ in solution. The spectra of different Ag-SWCNT dispersions for three different $AgNO_3$ concentrations are indicated in the same figure. Ag-SWCNT dispersion spectra are characterized by well-defined absorption features around 300 nm and a broad absorption band that starts around 400 nm and extends well above 800 nm. The absorption of the Ag-SWCNT dispersion increases with the $AgNO_3$ load. Optical absorption measurements on $AgNO_3$ solutions at room temperature or warmed to 470 K

without the SWCNT did not exhibit significant absorption in visible wavelengths. Thus, the observed optical absorption spectrum is attributed to the deposition of silver on the SWCNT surface.

3.3.2 Simulations of absorption spectra of spheres and elongated structures

Figure 2 illustrates simulations of the dependence of γ as a function of wavelength for elongated one-dimensional silver structures. For reference, the result of a simulation on a 10-nm silver sphere is illustrated on the figure. The spectrum is characterized by a band around 385 nm resulting from the excitation of the transverse plasmon mode in the spheres and a short wavelength tail that results from interband transitions.

The contribution of the longitudinal plasmon mode to the optical absorption spectrum is readily observed in the simulations corresponding to elongated silver nanostructures. The structures considered for the simulation have a length of 2,500 nm and diameters of 7, 500, and 2,000 nm. The structure of the absorption spectra is nearly insensitive to the diameter of the elongated nanostructure although the amount of light absorbed increases with the diameter of the structure at all wavelengths. The amount of light absorbed increases with wavelengths above 300 nm and extends to the near infrared in the spectra of the three elongated structures considered. The trend in light absorption toward long optical frequencies in elongated nanostructures is in marked contrast with those observed in spherical particles, a difference that results largely from the excitation of the longitudinal plasmon mode in the former nanostructures [12]. The extraordinary resemblance of the spectra discussed above with those predicted by the simulation

displayed in Figure 2 lead us to conclude that the optical absorption spectra of the Ag-SWCNT dispersion results from the formation of one-dimensional silver structures on the SWCNT.

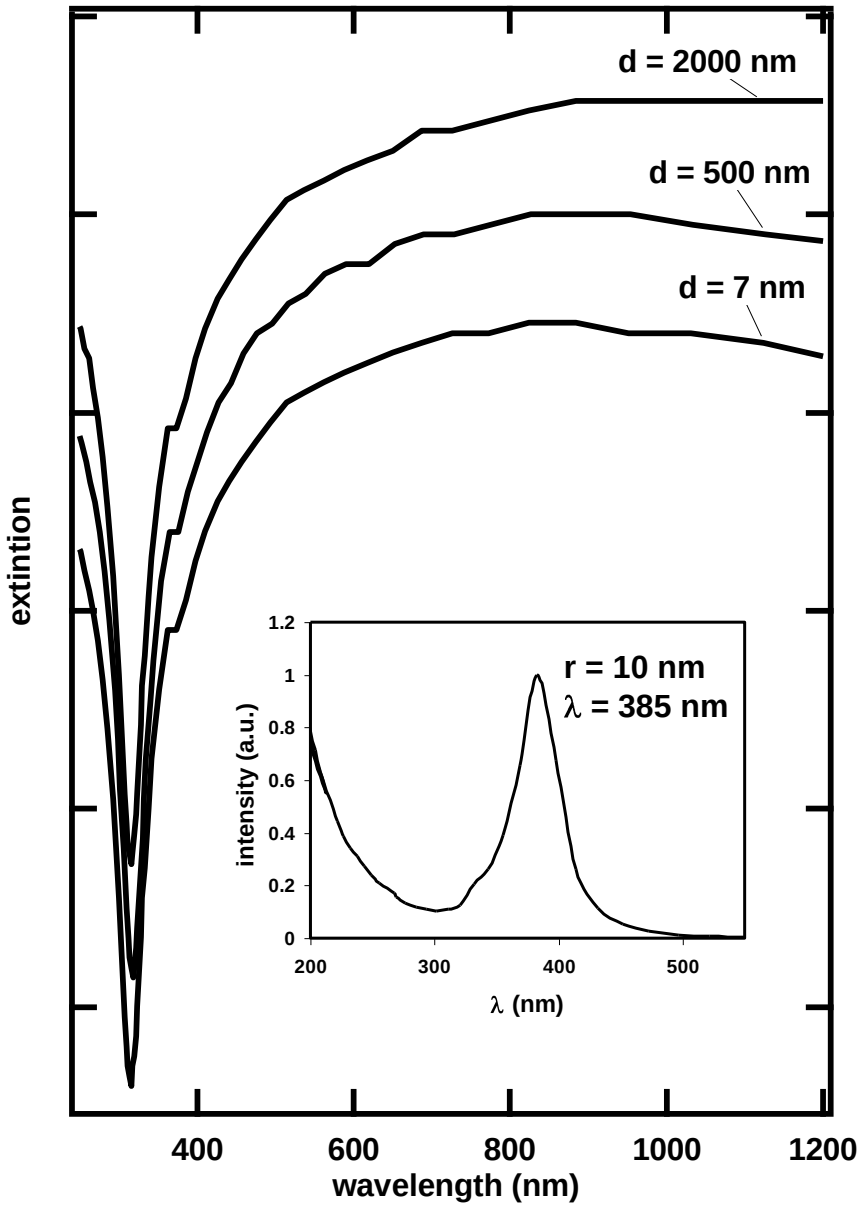

Figure 2. Dependence of the extinction coefficient. As a function of wavelength for one-dimensional silver structures with the indicated diameters (*d*) and a length of 2,500 nm. The insert illustrates the extinction coefficient of 10 nm silver spheres.

3.3.3 Characterization of Ag-SWCNT dispersions

Representative TEM and STM images of a dry deposit of the 1×10^{-5} M Ag-SWCNT dispersion are displayed in Figure 3. Well-dispersed SWCNT are readily identified in Figure 3a, consistent with the fine structure discussed in the context of the UV-visible absorption spectrum of the silver-SWCNT dispersion. Silver particles, about 30 nm in diameter, are formed while focusing the electron beam on the carbon grid used to support the sample. The diffraction pattern displayed on the inset of Figure 3a is consistent with an arrangement of polycrystalline silver atoms in the particle [17]. Figure 3b corresponds to the region in Figure 3a enclosed with a square. Particles that are about 7 nm in diameter, about three times the diameter of the 1.9 nm SWCNT, are readily observed. STM measurements of deposits prepared from the same 1×10^{-5} M Ag-SWCNT dispersion are displayed on Figure 3c. The STM images are consistent with the formation of one-dimensional silver nanostructures from the alignment of particle-like structures.

Dry deposits from samples with a larger silver content resulted in the formation of structures that required the use of the SEM for appropriate imaging. Figure 4 illustrates representative images of measurements performed on dry deposits of the Ag-SWCNT dispersions with an initial silver concentration of 1×10^{-2} M. The formation of dendrite-like structures shown in Figure 4a was common in the deposit. The smallest roughness features that we can spot in the image are shown in Figure 4b and have dimensions in the order of about 20 nm. Figure 4c shows EDAX mapping measurements of the same sample. It reveals well-defined regions containing silver, consistent with the deposition of silver on the SWCNT.

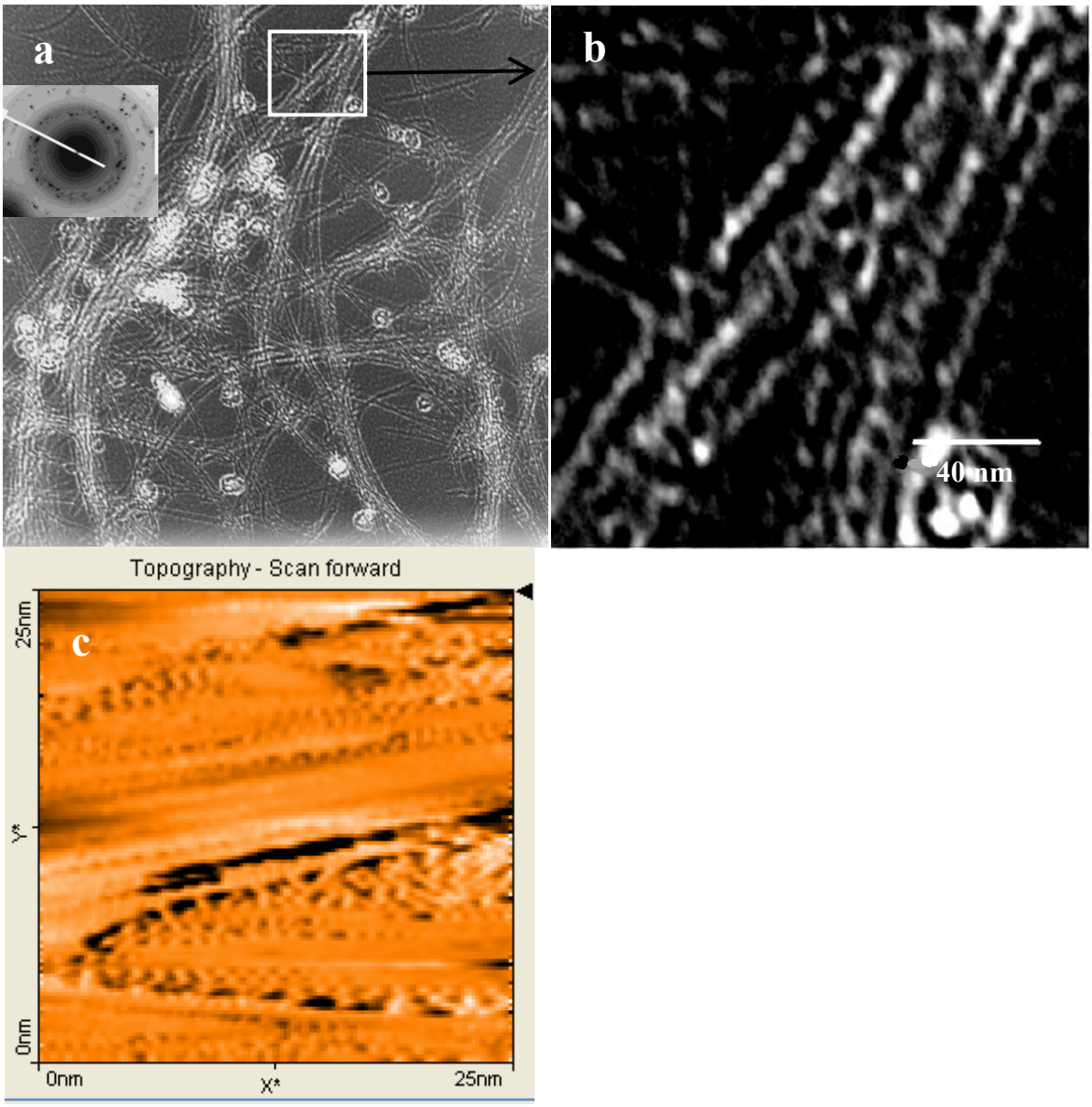

Figure 3. TEM images and STM image of Ag-SWCNT assemblies. The $AgNO_3$ concentration used for the preparation of the dispersion is 1×10^{-5} M. (a) Dispersed SWCNT and the silver diffraction pattern displayed in the insert, (b) 7 nm one-dimensional align silver particles, (c) STM image of Ag-SWCNT dry deposit.

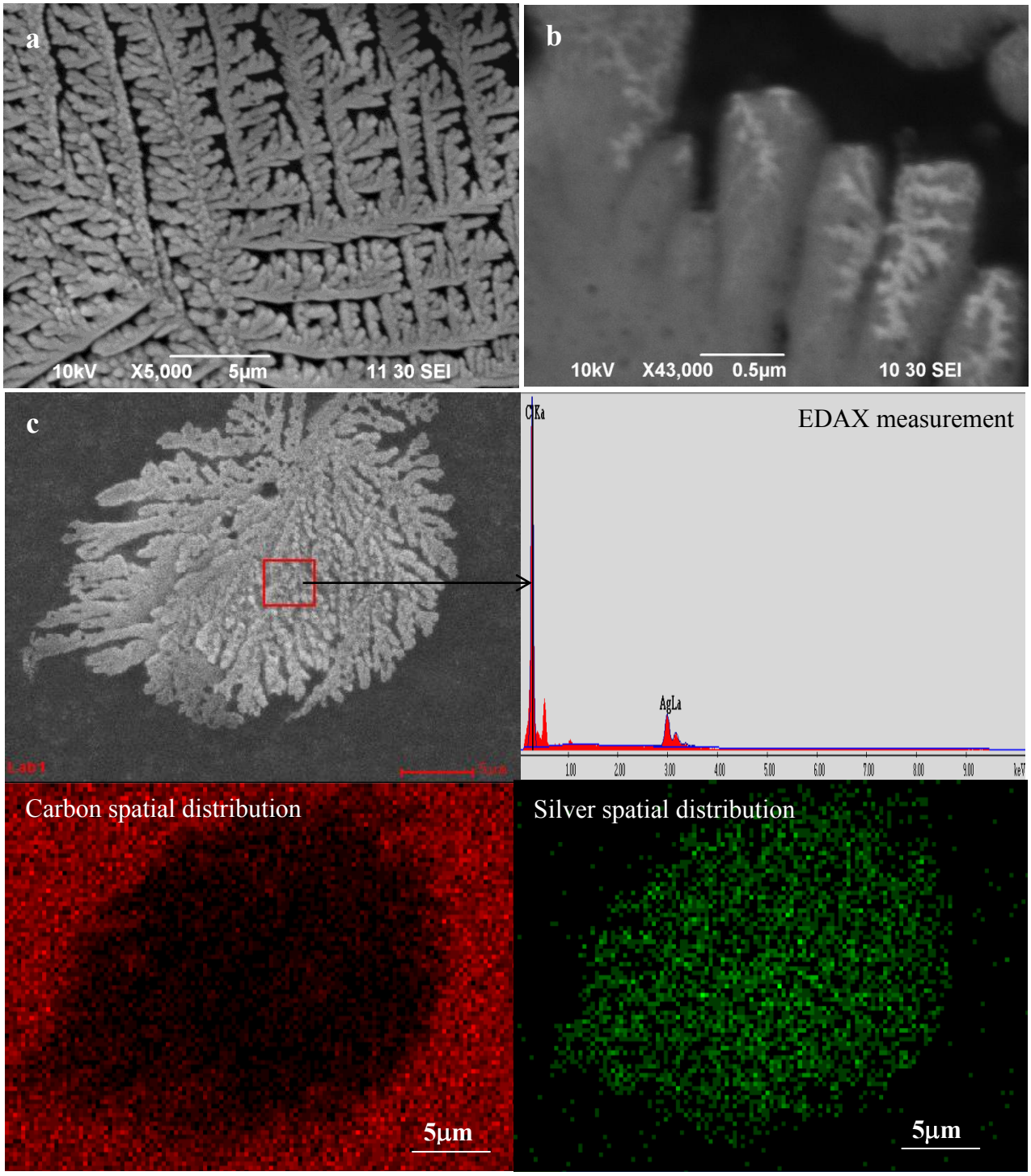

Figure 4. SEM and EDAX mapping measurement images of a Ag-SWCNT dispersion. With a $AgNO_3$ concentration of 1×10^{-2} M. (a) Dendrite-like structures, (b) smallest roughness features spotted in the sample, (c) EDAX mapping measurements.

3.4 Discussion

The imaging measurements performed on the SWCNT dispersions are consistent with the formation of one-dimensional silver nanostructures. The absorption spectra of all the Ag-SWCNT dispersions reported here have a similar structure, characterized by a significant increase in light absorption as the wavelength increases from UV to visible due to the excitation of the longitudinal plasmon mode. The simulations summarized in Figure 2, are consistent with the experimental UV-visible absorption measurements, as well as with the excitation of the longitudinal mode of silver nanostructures. Small differences between the simulated and experimental spectra likely rise from difference in the details of the morphology of the nanostructure: these differences are more notably between 300 and 400 nm, probably reflecting a small contribution arising from the transverse plasmon mode in silver. The simulations of the UV-visible absorption were performed on a silver film that is continuous in one dimension. The experimental evidence, particularly the TEM and STM images displayed on Figure 3, are consistent with the formation of discrete silver regions - about 7 nm wide - on the SWCNT surfaces. Electromagnetic coupling among these silver regions formed on the SWCNT surfaces could explain the observed light absorption spectra reported here. Sweatlock and coworkers performed theoretical calculations with the objective of establishing the contribution of the longitudinal plasmon mode to the absorption spectrum of one-dimensional arrays of 4, 8, and 12 spherical silver nanoparticles [18]. They reported that the longitudinal plasmon band shifted toward longer wavelengths with increasing the number of particles in a one-dimensional arrangement. Next neighbor distance was found to play an important role in

the predicted longitudinal plasmon absorption band, which was found to be inversely related to the particle-to-particle distance. Pinchuk and Schatz performed calculations on one-dimensional arrays of silver nanoparticles [19]. They found that the coupling of the electromagnetic field among silver nanoparticles arranged in one-dimensional arrays is sensitive to the particle-to-particle distance resulting in a broadening of the absorption band. Enoch et al. found that a small change in interparticle distance is enough to make a significant change in the absorption spectra: changes in interparticle distance smaller than 4 nm result in a red shift of the plasmon absorption band and a broadening of the absorption spectrum [20]. Near-field coupling of the electromagnetic field has also been reported by Maier [21], who found the dipole model adequate for electromagnetic energy transfer below the diffraction limit in chains of closely spaced metal nanoparticles. The spatial distribution of nanoparticles was found to play a role in electromagnetic coupling and the plasmon resonance band [22]. Unfortunately, we cannot establish a separation between these silver regions in a given nanotube from our measurements: in fact, the silver regions appear to be in contact in the STM image displayed on Figure 3c.

It could be argued that plasmonic nanoparticles also affect the optical properties of the carbon nanotubes. Indeed, Hanson has predicted that the presence of a plasmonic nanoparticle on a carbon nanotube wall affects the electric field and current on the carbon nanotube, and can be used to induce relatively large currents on the tube in the neighborhood of the sphere [23]. This view is consistent with recent experimental work. Sakashita reported the enhancement of photoluminescence intensity of single carbon nanotubes coupled to a rough gold surface. It was attributed to local field enhancement of

the incident light induced by localized surface plasmons [24]. However, the effect of plasmonic nanoparticles on the optical properties on SWCNT results in localized absorption in the neighborhood of the nanoparticle absorption plasmon wavelength, as opposed to the rather broad absorption spectra resulting from the excitation of the longitudinal plasmon mode observed here. In the case of silver nanospheres, the transverse mode is located between 300 and 400 nm. The significant structure found in the absorption spectra around 300 nm may result from the coupling predicted by Hansen, but further experimental work is necessary to establish the effect of plasmonic nanoparticles on the optical absorption spectrum of the SWCNT.

3.5 Summary

In summary, we have used single-wall carbon nanotubes (SWCNT) to template one-dimensional silver nanostructures. We observed evidence of the excitation of the longitudinal silver plasmon mode in the optical absorption spectra of Ag-SWCNT dispersions, even at the lowest silver concentrations employed. Tunneling and electron microscopy measurements are also consistent with the formation of one-dimensional silver nanostructures. The results indicate that silver deposits on SWCNT may be suitable candidates for light-to-energy conversion through coupling of the electric field excited in plasmonic particles.

3.6 References

1. Zhang G, Thomas JK: Radiation-induced energy and charge transport in polystyrene, laser photolysis and pulse radiolysis comparative study. Irradiation of Polymers, Chapter 3. 1996:28-54. ACS Symposium Series, Volume 620. Publication Date (Print): May 5, 1996 (Chapter).

2. Abkowitz MA, Stolka M, Weagley RJ, McGrane KM, Knier FE: Electronic transport in polysilylenes. Silicon-Based Polymer Science, Chapter 26. 1989:467-503. Advances in Chemistry, Volume 224. Publication Date (Print): May 5, 1989 (Chapter).

3. Aslan K, Leonenko Z, Lakowicz JR, Geddes CD: Fast and slow deposition of silver nanorods on planar surfaces. J Phys Chem B 2005, 109(8):3157–3162.

4. Maiyalagan T: Synthesis, characterization and electrocatalytic activity of silver nanorods towards the reduction of benzyl chloride. Appl Catalysis A Gen 2008, 340(2):191-195.

5. Pinchuk AO, Schatz GC: Nanoparticle optical properties: far- and near-field electrodynamic coupling in a chain of silver spherical nanoparticles. Mater Sci Eng B 2008, 149:251-258.

6. Maier SA, Brongersma ML, Kik PG, Atwater HA: Observation of near-field coupling in metal nanoparticle chains using far-field polarization spectroscopy. Phys Rev B, 65:193408.

7. Liu Y, Tang J, Chen X, Chen W, Pang GKH, Xin JH: A wet-chemical route for the decoration of CNTs with silver nanoparticles. Carbon 2006, 44(2):381-383.

8. Dai K, Shi L, Fang J, Zhang Y: Synthesis of silver nanoparticles on functional multi-walled carbon nanotubes. Mater Sci Eng A 2007, 465(1-2):283-286.

9. Lu G, Zhu L, Wang P, Chen J, Dikin DA, Ruoff RS, Yu Y, Ren ZF: Electrostatic-force-directed assembly of Ag nanocrystals onto vertically aligned carbon nanotubes. J Phys Chem C 2007, 111(48):17919-17922.

10. Harris1 N, Ford MJ, Mulvaney P, Cortie1 MB: Tunable infrared absorption by metal nanoparticles: the case for gold rods and shells. Gold Bull 2008, 41/1.

11. Iyer KS, Moreland J, Luzinov I, Malynych S, Chumanov G: Block copolymer nanocomposite films containing silver nanoparticles film formation, Chapter 11. 2006:149-166. ACS Symposium Series, Volume 941. Publication Date (Print): September 16, 2006 (Chapter).

12. Mayer ABR, Grebner W, Wannemacher R: Preparation of silver−latex composites. J Phys Chem B 2000, 104(31):7278-7285.

13. Naumov AV, Ghosh S, Tsyboulski DA, Bachilo SM, Weisman RB: Analyzing absorption backgrounds in single-walled carbon nanotube spectra. ACS Nano 2011, 5(3):1639-1648.

14. Bermudez VM: Adsorption on carbon nanotubes studied using polarization-modulated infrared reflection−absorption spectroscopy. J Phys Chem B 2005, 109(20):9970-9979.

15. Hartschuh A, Pedrosa HN, Peterson J, Huang L, Anger P, Qian H, Meixner AJ, Steiner M, Novotny L, Krauss TD: Single carbon nanotube optical spectroscopy. Chem Phys Chem 2005, 6:1-6.

16. Weisman RB: Optical spectroscopy of single-walled carbon nanotubes, Department of Chemistry, Center for Nanoscale Science and Technology, and Center for Biological and Environmental Nanotechnology. Houston: Rice University (To appear in: Contemporary Concepts of Condensed Matter Science, Volume 3 Elsevier).

17. Mandal S, Arumugam SK, Parisha R, Sastri M: Silver nanoparticles of variable morphology synthesized in aqueous foams as novel templates. Bull Mater Sci 2005, 28(5):503-510.

18. Sweatlock LA, Maier SA, Atwater HA, Penninkhof JJ, Polman A: Highly confined electromagnetic fields in arrays of strongly coupled Ag nanoparticles. Phys Rev B 2005, 71:235408.

19. Pinchuk AO, Schatz GC: Nanoparticle optical properties: far- and near-field electrodynamic coupling in a chain of silver spherical nanoparticles. Mater Sci Eng B 2008, 149:251-258.

20. Enoch S, Quidant R, Badenes G: Optical sensing based on plasmon coupling in nanoparticle arrays. Opt Express 2004, 12(15):3422.

21. Maier SA, Brongersma ML, Kik PG, Atwater HA: Observation of near-field coupling in metal nanoparticle chains using far-field polarization spectroscopy. Phys Rev B, 65:193408.

22. Negro LD, Feng N-N, Gopinath A: Electromagnetic coupling and plasmon localization in deterministic aperiodic arrays. J Opt A Pure Appl. Opt 2008, 10:64013.

23. Hanson GW, Smith P: Quantitative theory of nanowire and nanotube antenna performance. IEEE Trans Antennas and Propagation 2007, 55(11):3063-3069.

24. Sakashita T, Miyauchi Y, Matsuda K, Kanemitsu Y: Plasmon-assisted photoluminescence enhancement of single-walled carbon nanotubes on metal surfaces. Appl Phys Lett 2010, 97(6):63110.

Chapter 4

Functionalized Carbon Nanotubes-Myoglobin Interaction*

Proteins are large molecules that can adopt a variety of structural arrangements. A protein possesses a three-dimensional structure that is tied to its biological function. The present chapter focuses on the study of the interaction of the myoglobin protein with single-wall carbon nanotubes (SWCNT) and multi-wall carbon nanotubes (MWCNT) in aqueous solution. To achieve the protein-nanotubes interaction, the carbon nanotubes' surface modification was necessary. The results obtained suggest that there is indeed a protein-nanotube interaction.

**To be submitted*

4.1 Introduction

Myoglobin contains a single polypeptide chain and is relatively small (16,700 daltons) [1, 2]. It is an oxygen-binding protein that is found in muscle cells. Myoglobin was the first protein to have its structure determined by X-ray crystallography [3]; it is a globular protein. Globular proteins are usually very soluble in aqueous solutions; folded into compact units that are roughly spherical in shape. Myoglobin's tertiary structure consists of 8 α-helices which fold to make the compact globular protein. The folding occurs in such a manner that almost all of the hydrophillic groups are on the outside of the protein, facing the aqueous environment. Almost all the hydrophobic groups are inside the protein and the hydrophobic effect plays a large role in maintaining the stability of the folded protein [4]. Figure 1 shows a squematic representation of the myoglobin's active site, the heme group, in aqueous media. This group is responsible for the oxygen-binding properties of myoglobin. The protein surrounds the heme group, protecting the oxygen from release until the tissue needs it. As is shown in the representation, four nitrogen atoms are coordinated with the central Fe (II) atom. The Fe atom is coordinated on top by the proximal side chain of histidine and should be coordinated on the bottom with a diatomic oxygen molecule. In water, a free ferrous heme group can bind oxygen, but it only does so for a brief moment [5, 6]. The reason is that O_2 very rapidly oxidizes the Fe (II) to Fe (III), which cannot bind oxygen. This leaves a sixth ligation position, on the side of the heme plane opposite to the histidine. In aqueous solution, water molecules interact with this position. The heme iron is the binding site for ligands. The binding

occurs at the distal (from the histidine) side of the heme, the position occupied by the water molecule in the figure.

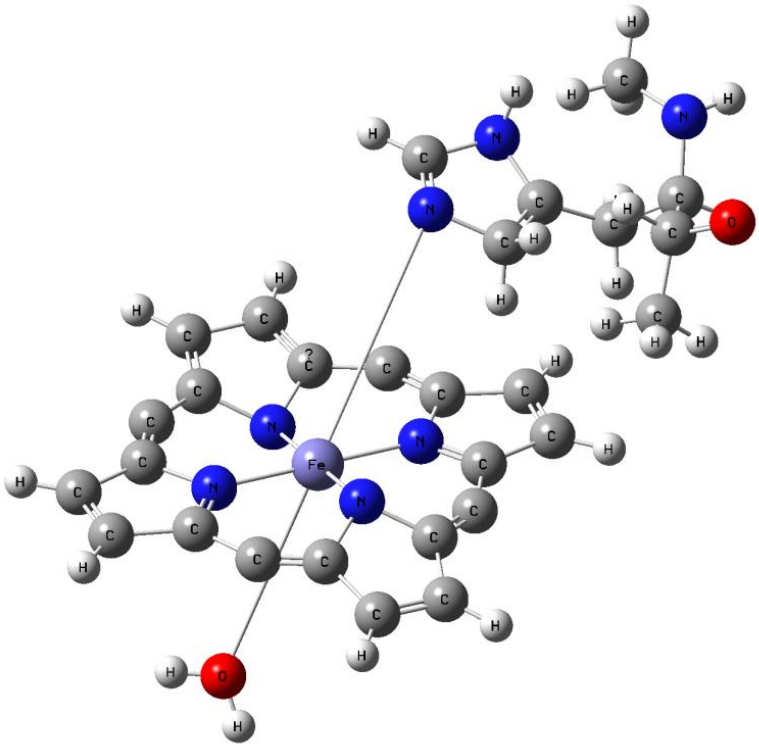

Figure 1: Squematic representation of the heme group

Actually, the carbon nanotubes modification has been the subject of numerous studies. Because of their unique mechanical, physical, and chemical properties, carbon nanotubes have great potential applications in many fields including molecular electronics, medical chemistry, and biomedical engineering [7-10]. Carbon nanotubes can be functionalized to achieve improved properties and functions such as biomedical capabilities [11, 12]. Functionalized nanotubes have potential sensing applications of several diseases. Cai et

al. reported that carbon nanotubes coated with a thin layer of protein-recognizing polymer form a biosensor capable of detecting minute amounts of proteins, which could provide a crucial new diagnostic tool for the detection of a range of illnesses [13]. They also reported that the carbon nanotubes biosensors are capable of detecting human ferritin, the primary iron-storing protein of cells, and the E7 oncoprotein derived from human papillomavirus, among other diseases. Also, further tests showed the sensor could discriminate between varieties of the protein that take different shapes. Liu et al. reported that protein-conjugated-nanotubes can cross cellular membranes and enter into the cell's body [14]. In this scenario, they can be filled with nucleic acids and be used as a delivery system for therapy genes or drugs.

The work presented here pursues the detection of myoglobin, an iron containing protein, in aqueous solution using surface modified SWCNT and MWCNT. Our interest in the detection of specifically this protein begins from the fact that it can be used for the identification of the rhabdomyolysis disease.

Myoglobin is a component of heart and skeletal muscles. When muscle tissue is damaged, the myoglobin in the muscle cells is released into the bloodstream [15]. The kidneys help remove myoglobin from the body. However, in large amounts, myoglobin can damage the kidneys. Possible complications of the disease include acute tubular necrosis and acute renal failure. Rhabdomyolysis is associated with high levels of the protein in the bloodstream. Under this condition, the muscle fibers breakdown, resulting in the release of the fiber contents, myoglobin, into the bloodstream.

To make a positive detection of this disease, it is necessary to carry out various analyses. These include: the verification of the levels of the creatinine phosphokinase enzyme, the myoglobin-serum, the potassium test, urinalysis and myoglobine urine among others. Some of these tests must be repeated for several days to obtain reliable results. In addition, the patient must monitor the consumption of medications and food during the study, since the results could be affected.

Studies by Grover et al. suggest that the accuracy and clinical utility of the assay used for the detection and diagnosis of rhabdomyolysis in patients has a poor and clinically inadequate sensitivity [16]. They conducted an analysis of the relationship between creatine kinase, serum-myoglobin, the urine qualitative assay for myoglobin and the semi-quantitative assay for urine pigments in patients evaluated for rhabdomyolysis. They found that that a negative test was not a result of the absence of the disease.

In order to achieve the interaction of myoglobin with nanotubes, the functionalization of the nanotubes with an amino group was necessary; since the nanotubes' functionalization makes possible the study of their interaction with the protein in aqueous solution. Obtained UV/Vis measurements suggest a protein-nanotubes interaction.

4.2 Experimental Section

4.2.1 Materials

The single (SWCNT) and (MWCNT) wall carbon nanotubes employed for the work described here were purchased from Cheap Tubes Inc. Myoglobin employed in the experiments described here is from esquine skeletal muscle, salt free and lyophilized and purchased from Sigma Aldrich. The initial protein concentration in the SWCNT and MWCNT dispersions in water studied here were 7.55×10^{-6} M and 1.32×10^{-5} M, respectively.

4.2.2 Equipment

UV-visible absorption measurements were conducted using a Jasco V-630 UV/Vis spectrophotometer. A quartz cuvette with an optical path of 0.25 cm was used for the optical absorption measurements. EDAX measurements were performed with the X-ray Fluorescent Detecting Unit of a JEOL 6480 LV Scanning Electron Microscope (SEM). EDAX measurements were performed on dispersions filtered with a 1 □m Whatson filter paper in a standard glass filter setup.

4.2.3 Carbon nanotubes functionalization

Samples of single-wall and multi-wall carbon nanotubes were functionalized with a carboxylic acid and amino terminal groups. The samples modified with carboxylic acid groups are represented as SWCNT-COOH or MWCNT-COOH, and the samples modified with amino groups are represented as SWCNT- NH_2 and MWCNT-NH_2. The

functionalization of the SWCNT and MWCNT was achieved following the procedure explained by B. Pan et al [17]**.** The chemical modification of the carbon nanotubes with amino terminals groups was verified by the appearance of vibrational bands around 1500 cm^{-1}. See Appendix B for the experimental data.

4.2.3.1 Preparation of SWCNT-COOH and SWCNT-NH_2

A 1.00 g amount of SWCNT was added to aqueous HNO_3 (10.0 mL, 60%). The mixture was placed in an ultrasonic bath for thirty minutes and then stirred for twenty-four hours while being boiled under reflux. The mixture was then vacuumed filtered through a 55mm filter paper and subsequently washed with distilled water until the pH of the filtrate was approximately 7. The filtered solid was dried from water at 100 °C. Dried SWCNT-COOH was suspended in $SOCl_2$ (20 mL) and stirred for eigth hours at 65 °C. The solution was filtered, washed with anhydrous THF, and dried from the $SOCl_2$ for two hours, generating SWCNT-COCl. The resulting solid was separated and subsequently washed with anhydrous THF. SWCNT-COCl was reacted with ethylenediamine to obtain SWCNT-NH_2.

Zhang et al. reported that the carbon nanotubes modified via the procedure used in our experiments contain some amine groups on the surface [18].

4.2.3.2 Preparation of MWCNT-COOH and MWCNT-NH_2

The MWCNT functionalization was achieved following the procedure explained for the SWCNT.

4.3 Results and Discussion

Figure 2 illustrates the dependence of the absorption spectra of myoglobin on time in the presence of (a) SWCNT-COOH and (b) MWCNT-COOH. The insert in each figure shows the maximum of the absorption band centered at 409 nm. These UV/Vis spectra are similar to the spectrum of myoglobin obtained in aqueous solution. Previous studies demonstrate that the most intense absorption band results from the interaction of the iron center with the protein body. This band is sensitive to changes in the coordination of the heme group. The signal at 502 nm is a Q band. The band with smaller intensity at 630 nm results from metal to ligand charge transfer. The spectra of dispersions containing the protein and the SWCNT-COOH and MWCNT-COOH do not exhibit any decrease in the intensity of the absorption band at 409 nm as a function of time, consistent with the absence of protein interactions with the carboxylic acid functionalized single or multi wall carbon nanotubes.

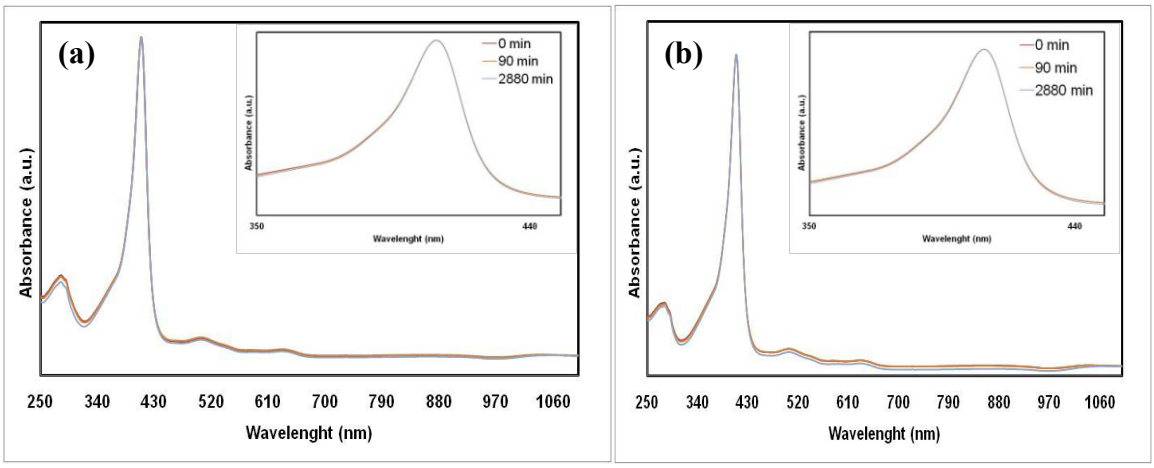

Figure 2: UV/Vis spectra showing the dependence of the myoglobin absorption on time in presence of (a) SWCNT-COOH and (b) MWCNT-COOH

Figure 3a and 3b summarizes the dependence of the absorption spectra of myoglobin on time in the presence of SWCNT-NH_2 and MWCNT-NH_2, respectively. The absorbance of the band centered at 409 nm decreases with time in the presence of the amine modified single or multi wall carbon nanotubes. The formation of a precipitate is readily observed during the interaction of the myoglobin and the dispersions of the carbon nanotubes modified with the amino group. The decrease in the 409 nm absorption band cannot be attributed to the protein denaturalization, since it is not observed when the myoglobin is mixed with the dispersion containing the carbon nanotubes functionalized with a carboxylic acid. Taken together, these observations lead us to conclude that the SWCNT-NH_2 or MWCNT-NH_2 remove the protein from the dispersion.

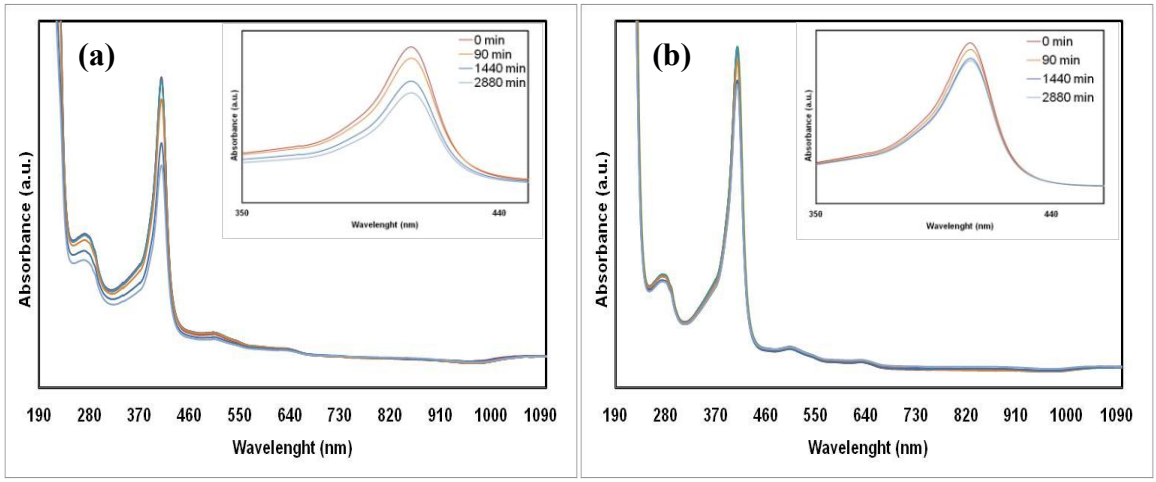

Figure 3: UV/Vis spectra showing the dependence of the myoglobin absorption on time in presence of water soluble (a) SWCNT-NH_2 and (b) MWCNT-NH_2.

EDAX measurements were performed with the purpose of characterizing the precipitate that results from protein-nanotubes interactions. The results are summarized in table1. Peaks due to the X-ray emission of carbon, oxygen, nitrogen and iron were found in the EDAX spectra of the precipitates. The strong background from the carbon support prevented the use of the carbon and oxygen and nitrogen peak areas for the interpretation of the results. On the other hand, the iron X-ray emission peak area found in the EDAX spectra of the precipitates obtained from the myoglobin/SWCNT-NH_2 and myoglobin/MWCNT-NH_2 dispersions increased by 1% and 6 % above a flat background signal. Figure 4 summarizes the iron peak area found in the myoglobin/SWCNT-NH_2 and myoglobin/MWCNT-NH_2 precipitates. The significant increase in iron X-ray emission peak leads us to conclude that the precipitates contain a significant amount of iron due to the precipitation of the amino functionalized carbon nanotube-myoglobin complex. Significantly, EDAX measurements on dry deposits obtained from filtered

dispersions of myoglobin/SWCNT-COOH and myoglobin/MWCNT-COOH do not exhibit any iron signal, indicating that the carboxylic acid functionality does not interact with the myoglobin.

Element	CK		NK		OK		FeK	
	Wt %	*At %*	*Wt %*	*At %*	*Wt %*	*At %*	*Wt %*	*At %*
SWCNT-NH_2	51.24	59.79	3.41	3.41	40.67	35.63	**4.68**	**1.17**
MWCNT-NH_2	62.03	78.98	3.39	3.71	11.48	10.98	**23.10**	**6.33**
SWCNT-COOH	70.72	76.01	3.63	3.35	25.53	20.60	**0.11**	**0.02**
MWCNT-COOH	70.72	76.02	3.63	3.35	25.53	20.60	**0.11**	**0.02**

Table 1: EDS quantitative results

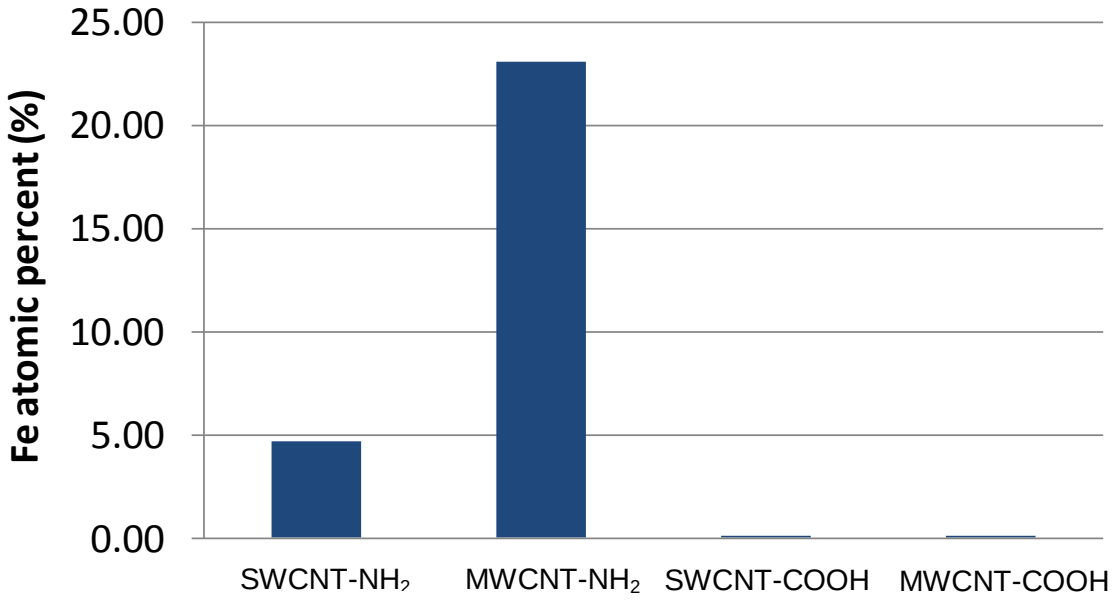

Figure 4: Iron atomic percent present on dry deposits of modified carbon nanotubes-protein solutions.

Figure 5a and 5b illustrates the amount of picked up by the carbon nanotubes modified with the amino group. The solid line is used to guide the eye through this discussion and does not represent a fit of the experimental data. The initial rate of protein removal by the SWCNT-NH_2 and MWCNT-NH_2 are 2.61 x 10^{-8} mmol/g and 2.46 x 10^{-8} mmol/gram respectively. Within the experimental uncertainty of our measurements, we conclude that the removal of myoglobin by the SWCNT-NH_2 and MWCNT-NH_2 is nearly independent of initial concentration over the range studied here.

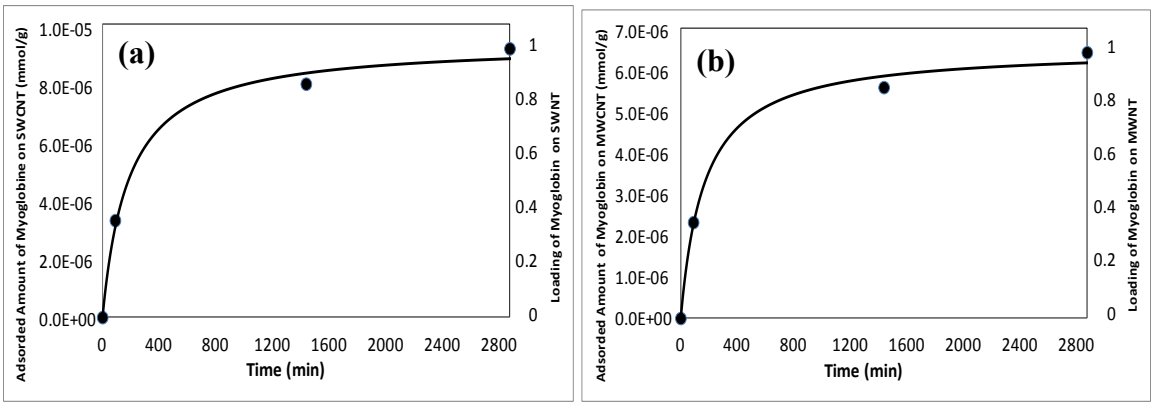

Figure 5: Dependence of the myoglobin absorption on time; (a) adsorbed protein amount on SWCNT-NH_2 and (b) adsorbed protein amount on MWCNT-NH_2.

It is difficult to establish the interactions between the functionalized carbon nanotubes and myoglobin that results in protein removal and the formation of a precipitate. It is likely that the amino group in the functionalized nanotubes interact with the hydroxyl groups the outer part of myoglobin. Alternatively, the amino group in the functionalized nanotube can interact with the iron atom in the heme center. Regardless, the formation of

a precipitate suggests that the interactions present are strong enough to make a sensor device for myoglobin in aqueous solution using amino terminated carbon nanotubes. In this regard it may be possible to develop nano- or microstructures that can pick up a single myoglobin molecule from solution and provide a quantitative measure of the protein in a sample. Changes in the oscillator frequency (ω) of well defined nano and microwires may be used as a quantitative measure of myoglobin in a patient. Such studies are beyond the scope of the present work, but represent an attractive and inexpensive approach to myoglobin detection in urine samples.

4.4 Summary

A clear interaction between the myoglobin protein and the aminated carbon nanotubes was suggested due to a decrease in the intensity of the band centered at 409 nm with time. The nanotubes modified with the carboxylic acid group, do not exhibit any decrease in the intensity of the absorption band at 409 nm in function of time, suggesting no protein-nanotubes interactions. The radical decrease of the myoglobin concentration in solution in presence of SWCNT-NH_2 suggests a more effective protein adsorption than the MWCNT-NH_2. Evidence in reduction of the myoglobin concentration in presence of SWCNT-NH_2 and MWCNT-NH_2, and the presence of a significant amount of iron in the dry deposits of the amine modified carbon nanotubes, suggest a possible detection of the protein in aqueous solution.

4.5 References

1. Lodish H, Berk A, Zipursky LS, Matsudaira P, Baltimore D, Darnell J : Evolutionary tree showing the globin protein family members myoglobin and hemoglobin, Molecular Cell Biology (4th ed.), 2000, W. H. Freeman.

2. Ordway GA, Garry DJ: Myoglobin: an essential hemoprotein in striated muscle, Journal of Experimental Biology 2004, 207 (Pt 20): 3441–6.

3. Kendrew JC, Bodo G, Dintzis HM, Parrish RG, Wyckoff H, Phillips DC: A Three-Dimensional Model of the Myoglobin Molecule Obtained by X-Ray Analysis, Nature 1958, 181 (4610): 662–6.

4. Hendgen-Cotta U, Kelm, M, Rassaf T: A highlight of myoglobin diversity: the nitrite reductase activity during myocardial ischemia-reperfusion, Nitric oxide: biology and chemistry / official journal of the Nitric Oxide Society, 2009, 22 (2): 75.

5. Goto Y, Takahashi N, Fink AL: Molecular dynamics simulations of isolated helices of myoglobin, *Biochemistry*, 1990, 29, 3480-3488.

6. Hirst JD, Brooks CL: 3rd Molecular dynamics simulations of isolated helices of myoglobin, Biochemistry, 34(23):7614–7621, June 1995.

7. Dalton AB, Collins S, Muñoz E, Razal JM, Ebron VH,. Ferraris JP, Coleman JN, Kim BG, Baughman RH: Super-tough carbon-nanotube fibres, Nature, 2003, 423, 703.

8. Haddon RC, Zanello LP, Zhao B, Hu H: Bone Cell Proliferation on Carbon Nanotubes, Nano Letters, 2006, 6 (3): 562–567.

9. Aliev AE, Oh J, Kozlov ME, Kuznetsov AA, Fang S, Fonseca AF, Ovalle R, Lima MD, Haque MH, Gartstein YN, Zhang M, Zakhidov AA, Baughman RH: Giant-Stroke, Superelastic Carbon Nanotube Aerogel Muscles, Science, 2009, 323 (5921): 1575-1578 .

10. Srivastava N, Banerjee K: Performance Analysis of Carbon Nanotube Interconnects for VLSI Applications, ICCAD, 2005, 383-390.

11. Zelada-Guillén G, Riu J, Düzgün A, Rius F: Immediate Detection of Living Bacteria at Ultralow Concentrations Using a Carbon Nanotube Based Potentiometric Aptasensor. Angewandte Chemie, 2009, 121, 7470–7473.

12. Villamizar RA, Maroto A, Rius F.X**:** Improved detection of *Candida albicans* with carbon nanotube field-effect transistors, Sensors and Actuators B: Chemical, 2009, 136, (2): 451-457.

13. Cai D, Ren L, Zhao H, Xu C, Zhang L, Yu Y, Wang H, Lan Y, Roberts MF, Chuang JH, Naughton MJ, Ren Z, Chiles TC.: A molecular-imprint nanosensor for ultrasensitive detection of proteins. Nature Nanotechnology, 2010, 5(8):597-601.

14. Liu Z, Tabakman S, Welsher K, Dai H: Carbon Nanotubes in Biology and Medicine: In vitro and in vivo Detection, Imaging and Drug Delivery, Nano Res, 2009 (2): 85-120.

15. O'Connor FG, Deuster PA. Rhabdomyolysis. In: Goldman L, Ausiello D, eds. Cecil Medicine. 23rd ed. Philadelphia, Pa: Saunders Elsevier; 2007: chap 114.

16. Grover DS, Atta MG, Eustace JA, Kickler TS, Fine DM: Lack of clinical utility of urine myoglobin detection by microconcentrator ultrafiltration in the diagnosis of rhabdomyolysis, 2004, 19 (10): 2634-2638.

17. Pan B, Cui D, Ozkan CS, Ozkan M, Xu P, Huang T, Liu F, Chen H, Li Q, He R, Gao F: Effects of Carbon Nanotubes on Photoluminescence Properties of Quantum Dots, J. Phys. Chem. C, 2008, 112, 939-944.

18. Zhang J, Zou H, Qing Q, Yang Y, Li Q, Liu Z, Guo X, Du Z: Effect of Chemical Oxidation on the Structure of Single-Walled Carbon Nanotubes, J. Phys. Chem. B 2003, 107, 3712-3718.

Chapter 5

Concluding Remarks

5.1 Thesis Contributions

Results of the first part of the research indicate that the optical absorption spectrum of carbon nanotubes is significantly affected by the presence of plasmonic nanoparticles. In particles, the absorption of light by SWCNT-Ag extends over a broader range of wavelengths. It is important since an improvement of the optical properties in SWCNT will likely result in various applications related to conversion of energy. These results also suggest that energy can be conducted through closely spaced one-dimensional arranged nanoparticles by means of the electric field generated by the excitation of plasmons.

Results of the second part of the research presented evidence in decrease of the myoglobin concentration as a function of time, in presence of SWCNT-NH_2 and MWCNT-NH_2. Myoglobin is an iron containing protein, and dry deposits of the amine modified carbon nanotubes showed a significant amount of iron. These results suggest a possible mode of detection of the protein in aqueous solution, and also suggest that the aminated nananotubes could function as sensors for the detection of myoglobin, the principal muscle fiber contents released into the bloodstream associated with the rhabdomyolysis disease.

5.2 Future Work

The work described in this document presents new possibilities for the use of one-dimensional plasmonic nanoparticles templated on SWCNT surfaces for energy applications. The use of these systems in areas related to the energy conversion, transportation, communication and manipulation surely will result in important future applications. SWCNT joined to a linear arrangement of silver nanoparticles can allow the transport of energy efficiently by the coupling of the electromagnetic fields of aligned metallic particles on its surface. Future work may focus in the improvement of the plasmonic response by examining different metallic nanoparticles adsorbed on nanotubes. Novel energy conversion applications are possible due to the manipulation of the direction and emission of light. After an optimization of the system, high efficient energy transport devices could be developed.

In biomedical applications, our results demonstrated that the myoglobin interaction with surface modified carbon nanotubes has the potential to become a biosensor for the diagnostic of the rhabdomyolysis disease. Future works can be focused in the study of the interaction of this biosensor with other proteins present in biological fluids, in order to validate our system's selectivity as well as improvements in the system response time.

Appendix A

A cybernetic portal to science and engineering education: vibrational spectroscopy of organic molecules

A.1 Introduction

This section presents a description of a laboratory activity developed for the undergraduate organic chemistry course. The activity aims to strengthen the knowledge of students in organic chemistry concepts by developing an active learning activity. Based in educational research data, students learn passively or actively. In passive learning, people are just information receptors, but thru active learning people are conducted to think about what they are doing [1].

Activities that promote active learning facilitate students achieve a high level of engagement with their courses [2]. Student exposed to hands on activities as a learning mechanism are more likely to recall information later and use it in different contexts [3]. Over the years, educators have been encouraged to add active learning experiences to their daily teaching activities at the college and high school levels with the purpose of improving science and engineering learning. There are various forms of active learning discussed in the literature. The forms of active learning include discovery learning, problem-based learning, experiential learning, and inquiry-based instruction [4].

Laboratory activities play a central role in science and engineering learning and are typically used as a mechanism to bring fundamental concepts to students. Indeed, laboratory activities are a mechanism of active learning that relies on experimental learning. These are unique activities, where students experiment with knowledge themselves instead of hearing or reading about the experiences of others. Instructors play a central role in facilitating the integration of concepts and theory by students thru laboratory experiences.

Educational research classifies learning in different levels and styles [5, 6]. Learning levels in chemistry are classified as macroscopic, microscopic and symbolic. Macroscopic learning level relies on tangible and visible phenomena while microscopic learning level provide explanation at a level that is invisible to the naked eye and requires the use of student imagination. Symbolic learning level, on the other hand, represents

processes in term of formulas and equations [5]. Most chemistry concepts are represented at the symbolic level. In this level, students relate macroscopic observations with microscopic explanations. It has been well documented that many students have difficulty understanding chemical phenomena at the microscopic level [8-18]. Students must be exposed to experiences that can facilitate the relation of fundamental concepts with real observations.

Chemistry students interact with new information at the symbolic level, and then they construct their own informal mental modes to facilitate the material understanding. Students describe their models at the symbolic level using words, equations, pictures, diagrams, or a combination of these. A complete experimental experience is necessary to enable students to develop a correct mental model of the presented material in a typical chemistry lecture.

Individualized learning styles are also important in achieving good understanding by students. A learning style is the method of learning of a particular person. It is presumed to allow that person to learn best. It has been proposed that educators should assess the learning styles of their students and adapt their classroom methods to best fit each student's learning style. Basic learning styles are classified as: visual learning (learn by seeing), auditory learning (learn by hearing) and kinesthetic or practical learning (learn by doing) [19, 20]. Laboratory activities should be designed and presented embracing all the basic learning styles.

Unfortunately, not all academic institutions, colleges and high school included, have instrumentation suitable for the multiple teaching tasks in chemistry curriculum. This has limited hands-on chemistry learning to reach all education levels. To achieve this objective we could take advantage of the technology available in other institutions. A technological tool with this intention has been developed. It allows students to perform laboratory experiments in real time by accessing thru the internet, state-of-the-art instrumentation not physically available in their laboratory classroom. This PC to PC communication tool enables students to keep interest in chemistry concepts. They can be trained in the use of specialized instrumentation and furthermore, the entire laboratory group could be impacted at the same time. We have called this a cybernetic approach "Portal to Science and Engineering Education". A concept representation is shown in figure 1.

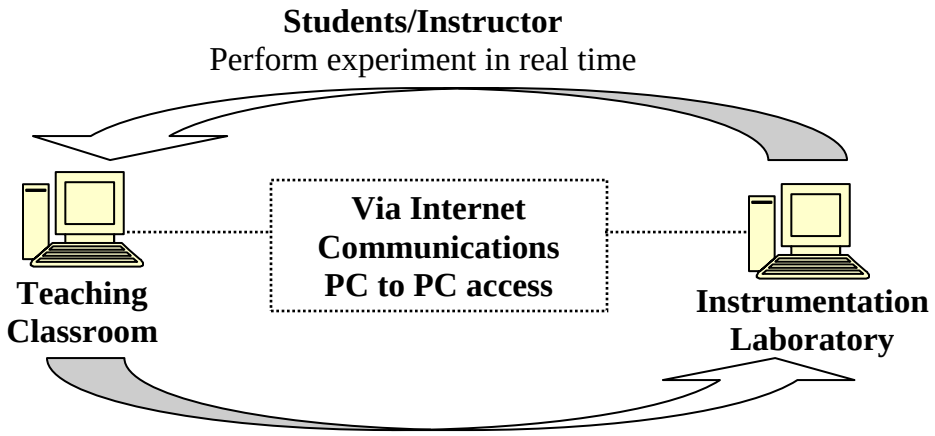

Figure 1: Representation of the "Portal to Science and Engineering Education" concept

A portal can facilitate the achievement of all learning styles. Visual learning students can associate ideas, concepts and data with real images represented graphically. Auditory

learners, on the other hand, can benefit from the focused explanation of an instructor while data is acquired in real time. The kinesthetic or practical learning is achieved by means of the instrument manipulation from a computer in the teaching classroom and the sample preparation. A portal to science and engineering education takes advantages of PC to PC communication tools to facilitate the implementation of these different learning styles. Chemistry laboratory course work can benefit of such activities by allowing student access to instrumentation that can enable the observation of a number of properties in matter, and from atoms to measurements of optical absorption and emission properties.

In organic chemistry, compounds are classified by their molecular structural arrangement or functional groups. A typical course emphasizes the importance to recognize the different organic compounds and predict chemical properties and reactions. In the undergraduate laboratory, the introduction to spectroscopy techniques for the characterization of organic compounds by the identification of functional groups in molecules is included in the curriculum. For this purpose, the Fourier transform infrared spectroscopy (FTIR) technique is introduced as material of study in the course. It is important for teachers and students to have hands on experiences in such techniques with the purpose of fulfilling their learning styles. The high acquisition and maintenance costs associated with FTIR instruments prevent their common use in small colleges and high schools. Access to internet, on the other hand, is now days common in must colleges and in high schools. Generally, the material discussion is purely theoretical in these courses in the absence of an instrument to apply the acquired knowledge about a

technique. For the implementation of the activity described here, simple FTIR experiment was designed and implemented. The experiment uses PC to PC access technology via internet to bring to students a hands-on experience with instrumentation available in other institutions. In this experiment the students obtained experimental results in real time and had complete instrument manipulation from a computer in their teaching classroom. The contribution that we will make with this science portal activity is focused on the interaction of light with matter, and in the context of the organic chemistry course work, the identification of different functional groups.

A.2 Activity description

The organic chemistry laboratory was chosen to develop Science Portal in spectroscopy. The subject of different functional groups is ideally suited for a hands-on experience. The experimental group, selected randomly, consists of sixteen organic chemistry laboratory students. The group was composed of chemistry and biology mayors. The students were placed in groups of four. Each group shared a common table. A typical teaching laboratory equipped with a Smart Board (*Audiovisual Concept Company*) and wired internet access was employed for the activity described. The Smart Board allowed the group to appreciate the experiment in progress in real time from any location in the classroom. A picture of the teaching classroom taken during the laboratory experiment is presented in figure 2. The laboratory objective is the identification of functional groups in organic chemistry compounds by FTIR spectroscopy.

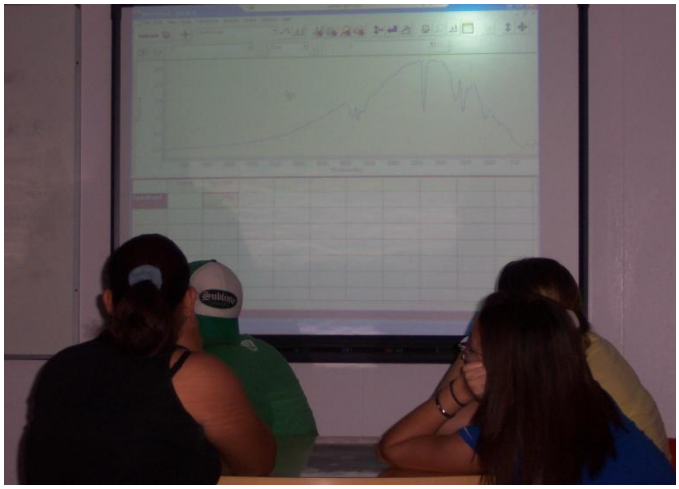

Figure 2: Students participating in a PC to PC activity using the smart board at UPR Ponce using an FTIR instrument at UPR Mayaguez

The first part of the experiment includes a discussion of the fundamental concepts associated with the FTIR technique. Furthermore, students got familiarized with correlation tables and examples of spectra of different organic compounds. A description of the FTIR spectrometer used was presented. Pictures from the instrumentation used and the research laboratory were shown. The type of cells used and the difference in cells materials were also discussed. The identification of organic compounds by the technique, specifically the compounds classification by functional groups was the purpose of the discussion. The changes caused in the rotational and vibrational states of molecules by the energy absorption, the wavelength of the electromagnetic radiation that comprises the IR region and units, were among the concepts discussed. The importance and information provided by the different regions of the infrared range were also discussed. Figure 3 illustrate how the laboratory activity was developed.

Figure 3: Laboratory activity developed

The second part of the experiment focuses on sample preparation. The compounds to be analyzed, methanol and acetone, were chosen in order to demonstrate the diverse chemical behavior of the different organic compounds. Students prepared a sample equal to the one to be analyzed in the FTIR spectrometer. In the laboratory where the instrument is located, a graduate student placed the sample in the FTIR spectrometer compartment. The methodology of the experiment operation, the background collection and sample measurement were presented in real time. In this part of the experiment, students got total access of the instrumentation from the computer in the teaching classroom. Once the data of the two compounds, methanol and acetone, was acquired, the compounds were classified by the students in a discussion of bands region assignment.

A.3 FTIR manipulation

To access the computer's FTIR from the teaching classroom, the *Remote Desktop Connection* accessory of the Windows XP operating system was used. The accessory permits to connect to a computer's desktop from a remote location, and run applications as if you were sitting at its console. From the teaching classroom the computer's

instrument was accessed following the steps presented in figure 4. After the procedure we got total control of the FTIR computer.

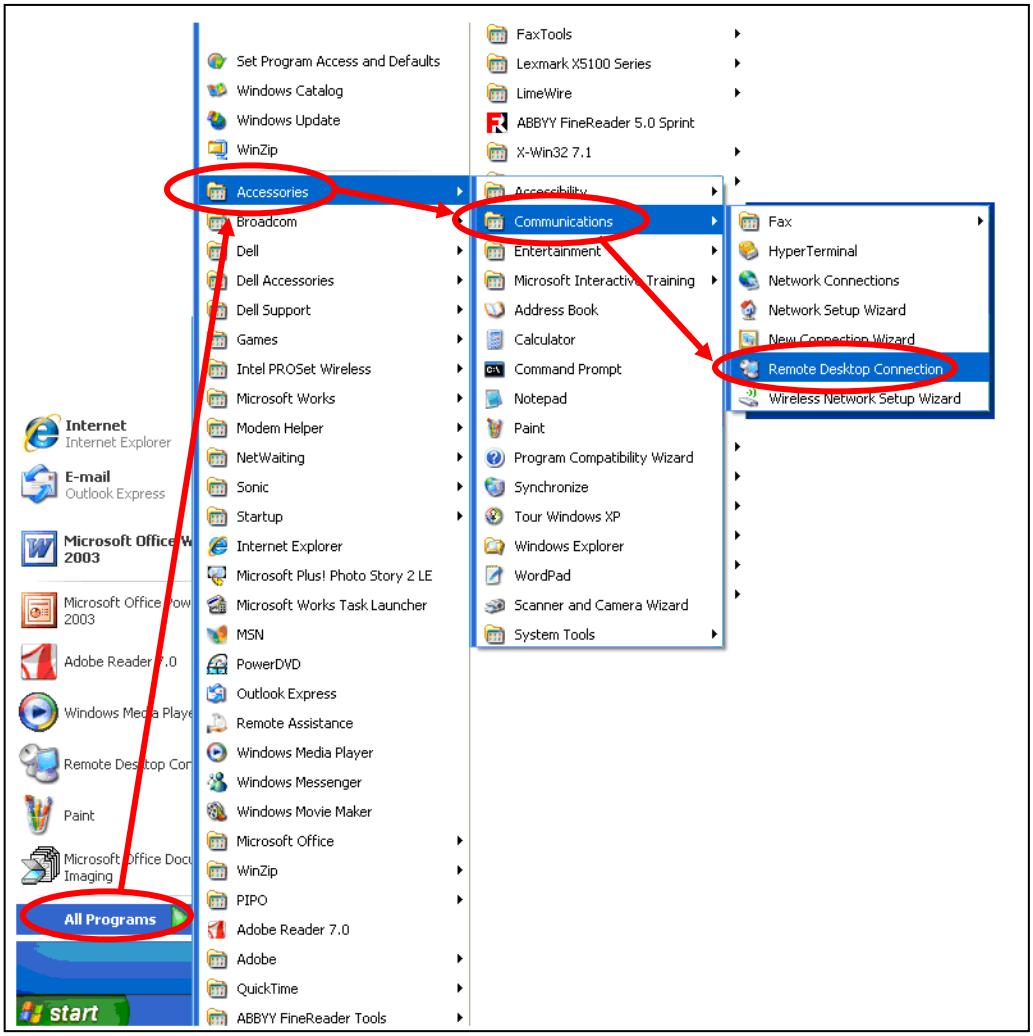

Figure 4: The computer's instrument was accessed from the computer's teaching classroom by pressing: START, ALL PROGRAMS, ACCESSORIES, COMMUNICATIONS, REMOTE DESKTOP CONNECTION, and writing the computer's instrument IP address

A.4 Assessment: Students' impact

There was a general improvement in student average in the organic chemistry exam related to spectroscopy as compared to the previous year. Before the exam, of the 16 students initially registered, 3 dropped the course. Last year the average in the exam was 67%, while this year the average increased to 81%. The type and number of text questions were the same in both years. Students explicitly informed to the professor on the success of the approach in bringing a hands-on experience to the organic chemistry laboratory in the area of spectroscopy. The increase in exam average grade also evidences the impact of the activity in assisting a teacher introducing organic chemistry concepts in the classroom.

A.5 References

1. McManus Dean A. Journal of Geoscience Education,Vol. 49, No. 6, Nov 2001, pp. 423-434.

2. Biggs, John. Teaching for quality Learning at University, Second Edition, Open University Press, McGraw-Hill Education, Maidenhead, Berkshire, UK, 2003.

3. Bruner, J. S. (1961). "The act of discovery". Harvard Educational Review 31 (1): 21–32.

4. Kirschner, P. A., Sweller, J., and Clark, R. E. (2006). "Why minimal guidance during instruction does not work: an analysis of the failure of constructivist, discovery, problem-based, experiential, and inquiry-based teaching". Educational Psychologist 41 (2): 75-86.

5. Jonhstone, A.H. (1991). Why is science difficult to learn; things are seldom what they seem. Journal of Computer Assisted Learning, 7, 75-83.

6. Sodhi Gurvinder S., Kaur Jasjeet. Journal of chemical education, Vol 76, No.4, April 1999.

7. Hinton Michael E., Nakhleh Mary B., Chem. Educator, 1999, 4, 158-167.

8. Hornby Michael, Peach Josephine, Journal of Chemical Education, Vol. 80 No. 2, February 2003.

9. Sanger, Michael J. J. Chem. Educ. 2005**,** Vol. 82 No. 1, 131

10. Lythcott, Jean. J. Chem. Educ. 1990, 67, 248–252.

11. Nakhleh, Mary B. J. Chem. Educ. 1992, 69, 191–196.

12. Smith, Kimberly Jo.; Metz, Patricia A. J. Chem. Educ. 1996, 73, 233–235.

13. Ebenezer, Jazlin V.; Erickson, Gaalen L. Sci. Educ. 1996, 80, 181–200.

14. Lee, Kam-Wah Lucille. J. Chem. Educ. 1999, 76, 1008–1012.

15. Sanger, Michael J. J. Chem. Educ. 2000, 77, 762–766.

16. Raviolo, Andrés. J. Chem. Educ. 2001, 78, 629–631.

17. Mattox Adam C., Reisner Barbara A., Rickey Dawn, Journal of Chemical Education, Vol. 83, No. 4 April 2006.

18. Dunn, R., Dunn, K., & Price, G. E. (1984). Learning style inventory. Lawrence, KS, USA: Price Systems

19. Coffield, F., Moseley, D., Hall, E., Ecclestone, K. (2004). Learning styles and pedagogy in post-16 learning. A systematic and critical review. London: Learning and Skills Research Centre

Appendix B

Carbon nanotubes functionalization

Because of their unique mechanical, physical, and chemical properties, carbon nanotubes have great potential applications in various fields including molecular electronics, medical chemistry, and biomedical engineering. Carbon nanotubes can be functionalized to achieve improved properties and functions such as biomedical capabilities. Protein-conjugated-carbon nanotubes can cross the cellular membrane and enter into the cytoplasm and cell nucleus. In this scenario, they can be filled with nucleic acids and be used as a delivery system for therapy genes or drugs (*J. Phys. Chem. C* **2008,** *112*, 939-944).

B.1 Preparation of SWCNT-COOH and SWCNT-NH_2

A 1.00 g amount of SWCNT was added to aqueous HNO_3 (10.0 mL, 60%). The mixture was placed in an ultrasonic bath for thirty minutes and then stirred for twenty-four hours while being boiled under reflux. The mixture was then vacuumed filtered through a 55mm filter paper and subsequently washed with distilled water until the pH of the filtrate was approximately 7. The filtered solid was dried from water at 100 °C. Dried

SWCNT-COOH was suspended in $SOCl_2$ (20 mL) and stirred for eigth hours at 65 °C. The solution was filtered, washed with anhydrous THF, and dried from the $SOCl_2$ for two hours, generating SWCNT-COCl. The resulting solid was separated and subsequently washed with anhydrous THF. SWCNT-COCl was reacted with ethylenediamine to obtain SWCNT-NH_2.

B.2 Preparation of MWCNT-COOH and MWCNT-NH_2

The MWCNT functionalization was achieved following the procedure explained for the SWCNT.

B.3 SWCNT characterization

UV/Vis and FTIR was employed in verifying the carbon nanotubes functionalization. Figure B.3.1 shows the absortion spectra for the assynthesized SWCNT and the functionalized SWCNT-COOH. This functionalization was achieved from the SWCNT's exposition to nitric acid solution, as explained in section B.1. The figure shows a considerable difference in the absorption signals. As was previously mentioned, carbon nanotubes posees a polyaromatic surface. In systems like these, any substance causes a primary band shift to longer wavelengths. The shoulder at approximately 225 nm in the assynthesized SWCNT (As-syn) spectrum was shifted to 280 nm after adding the COOH group, an auxocrome. This group extends the system conjugation due to a batocromic effect, caused by resonance.

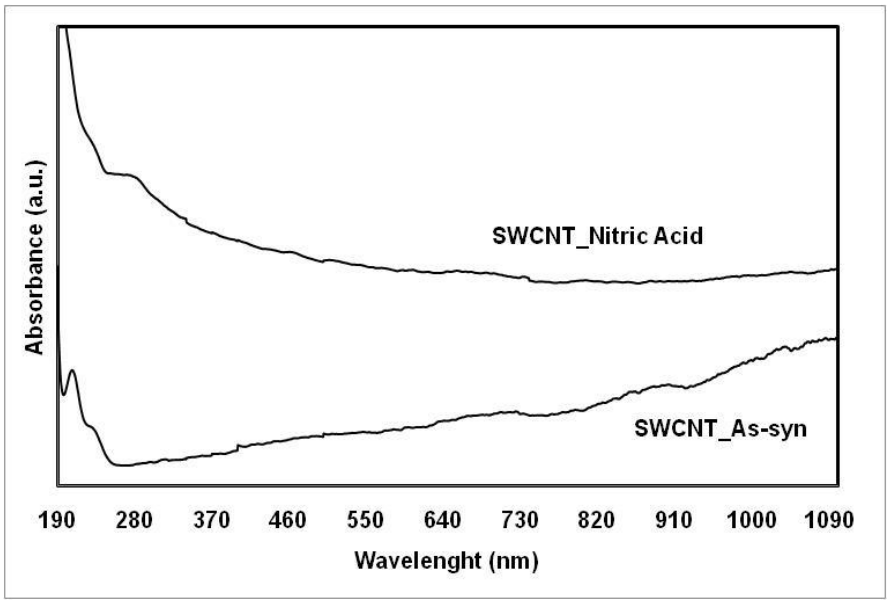

Figure B.3.1: Absortion spectra for the assynthesized SWCNT and functionalized SWCNT-COOH.

Figure B.3.2 shows the effect of change OH by Cl in the SWCNT structure. When Cl replaces the OH group, the shoulder signal at approximately 280 nm in the SWCNT-COOH spectrum is a little shifted to smaller wavelengths in SWCNT-COCl. This hipsocromic effect could be attributed to the inductive effect exerted by Cl.

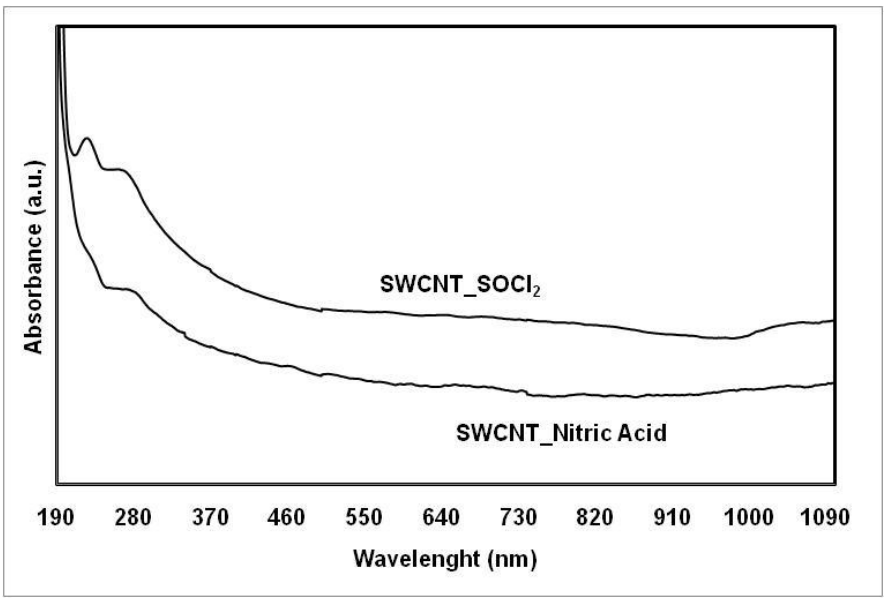

Figure B.3.2: Effect of the change of OH by Cl in the SWCNT structure.

Figure B.3.3 shows the SWCNT-Cl and SWCNT-NH_2 spectra. Due to the broadening of the SWCNT-NH_2 signal, a specific shift in SWCNT-Cl signals could not be appreciated. This might be attributed to the substitution of Cl by NH_2, both of them auxocromes. Both electronegative groups exert inductive effects in the carbonyl lone pairs, causing a stronger attraction of these electrons by the oxygen atom in the carbonyl group.

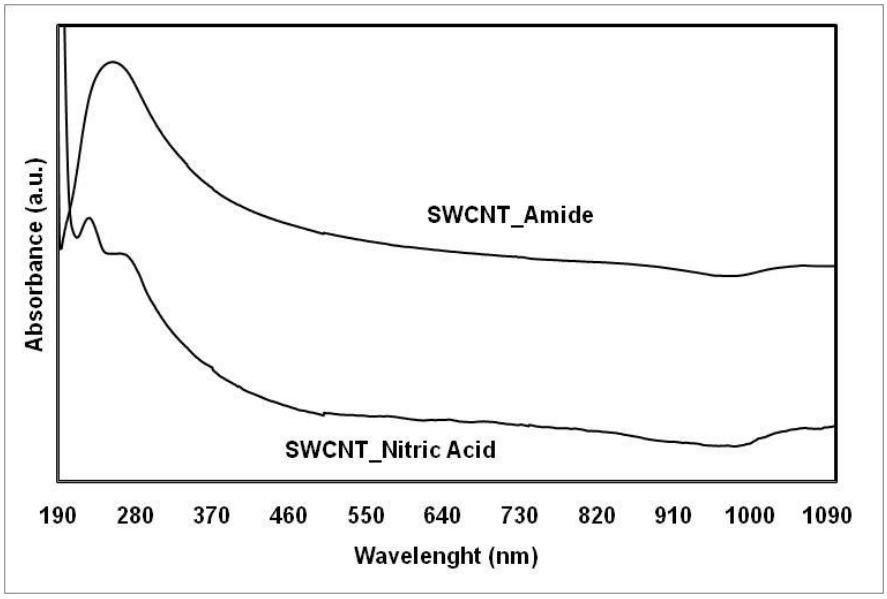

Figure B.3.3: SWCNT-Cl and SWCNT-NH_2 spectra.

Figure B.3.4 summarizes the signals changes before and after the SWCNT amidation. A clear change can be observed after the process, suggesting the formation of SWCNT-NH_2.

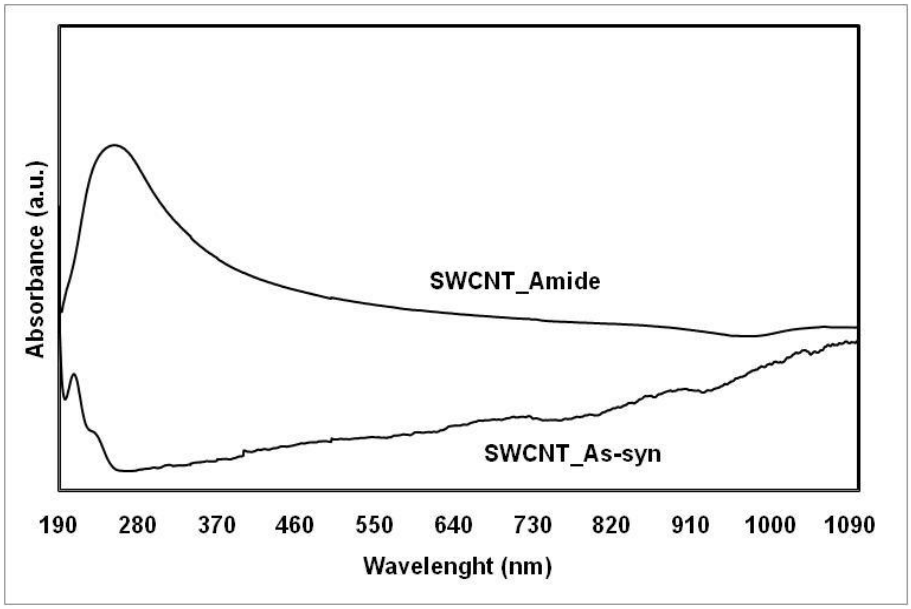

Figure B.3.4: Signals before and after the SWCNT functionalization.

The FTIR spectra of the assynthesized and functionalized SWCNT are shown in figure B.3.5. A signal due to N-H vibrations in SWCNT-NH_2 could be appreciated in the corresponding spectrum.

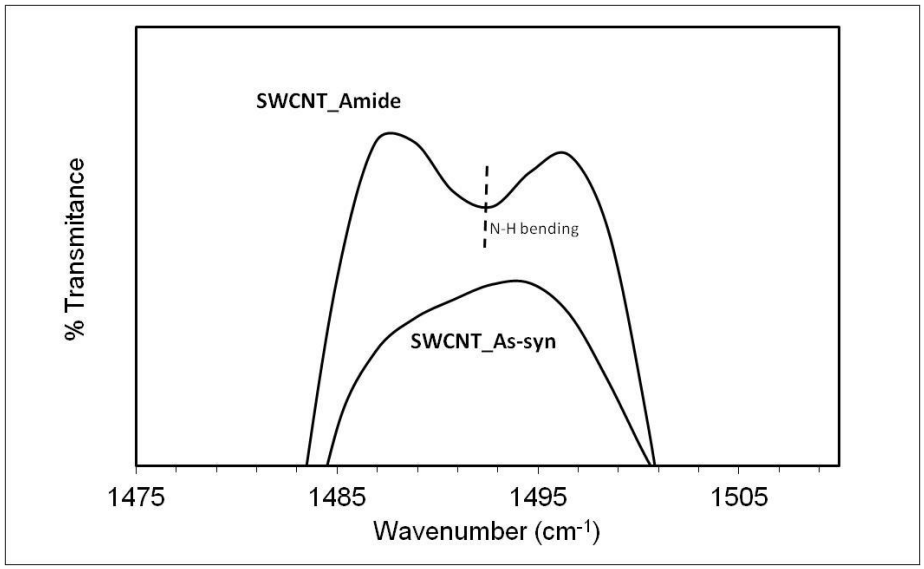

Figure B.3.5: The FTIR spectra of the assynthesized and functionalized SWCNT.

Before and after the functionalization procedure, the Raman spectrum of the assynthesized SWCNT and SWCNT-NH_2 samples displayed in Figures B.3.6 and B.3.7 respectively, shows that the nanotubes conserved its framework, since its characteristic signals are maintained after the process.

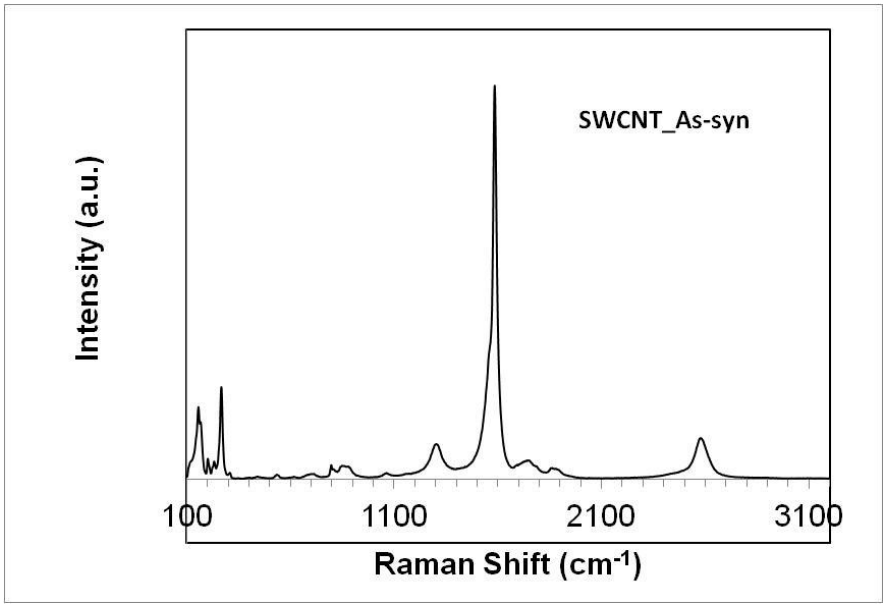

Figure B.3.6: Raman spectrum of SWCNT-Assynthesized.

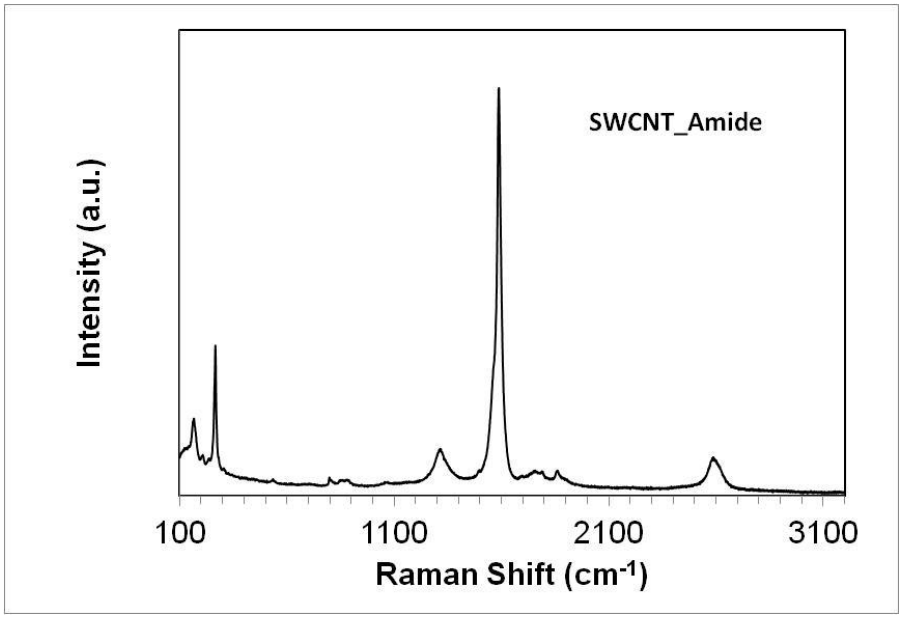

Figure B.3.7: Raman spectrum of SWCNT-NH_2.

B.4 MWCNT characterization

Results obtained from the MWCNT functionalization are similar to the ones obtained with the SWCNT. Figure B.4.1 shows the batocromic effect due to the COOH group, also observed in the same step with the SWCNT.

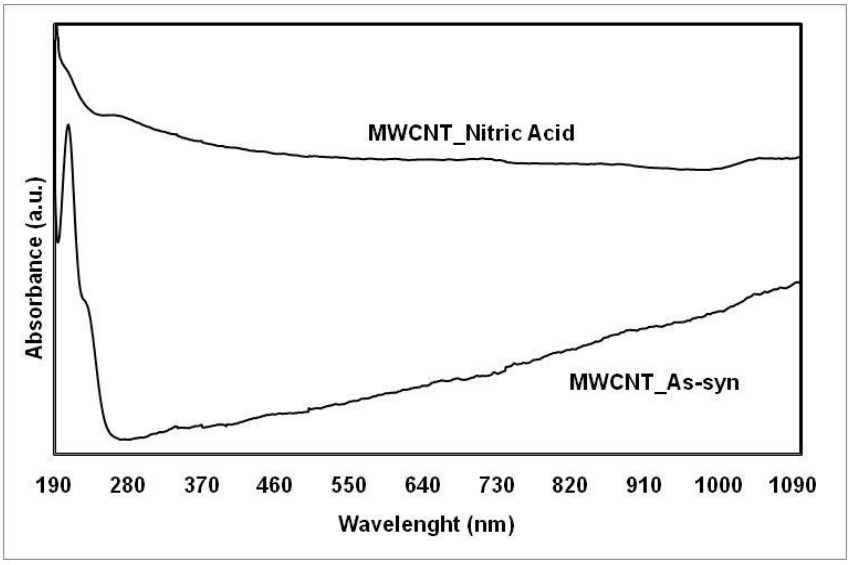

Figure B.4.1: Absortion spectra for the assynthesized MWCNT and functionalized MWCNT-COOH.

Figure B.4.2 shows the effect of the change of COOH by Cl.

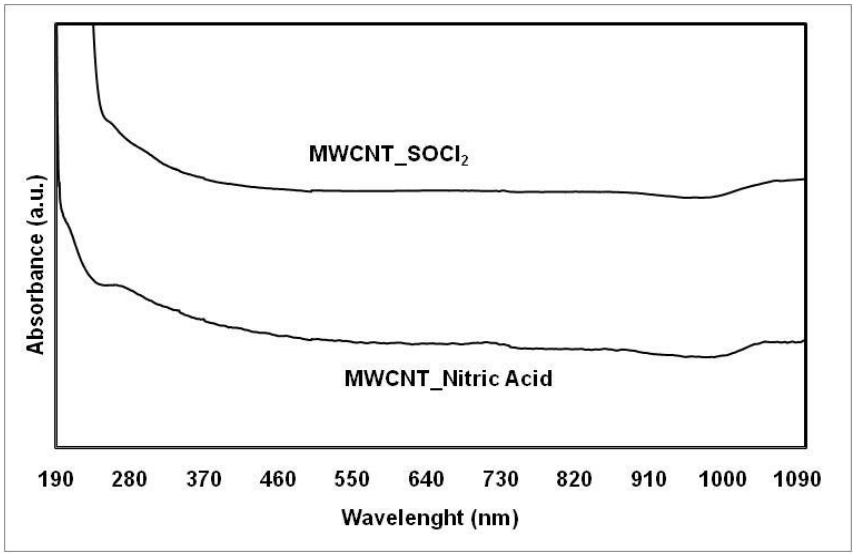

Figure B.4.2: Effect of the change of OH by Cl in the MWCNT structure.

Figure B.4.3 shows a signal broadening in MWCNT due to the substitution of Cl by NH_2, also observed with the same procedure in the SWCNT.

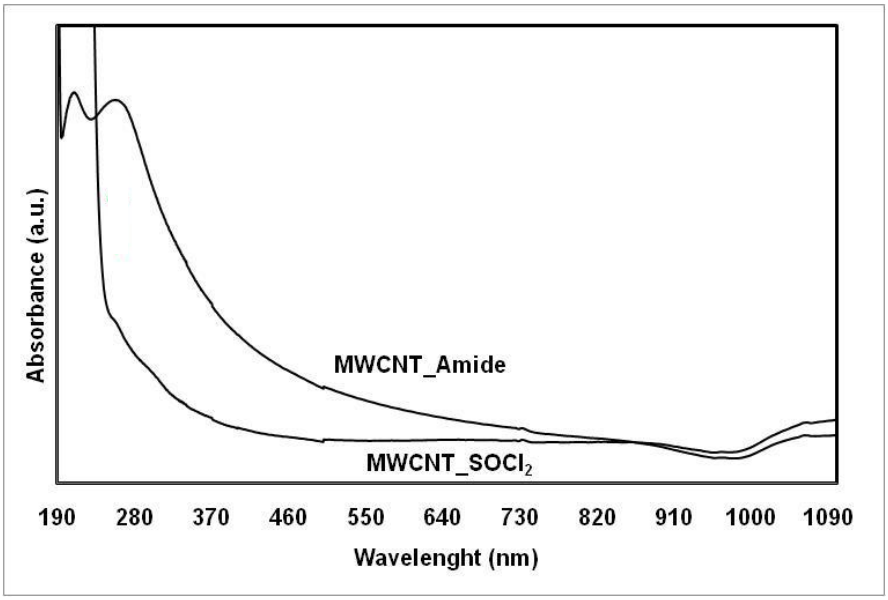

Figure B.4.3: MWCNT-Cl and MWCNT-NH_2 spectra.

Figure B.4.4 summarizes the change in the asynthesized MWCNT and MWCNT-NH_2, suggesting the nanotubes amidation.

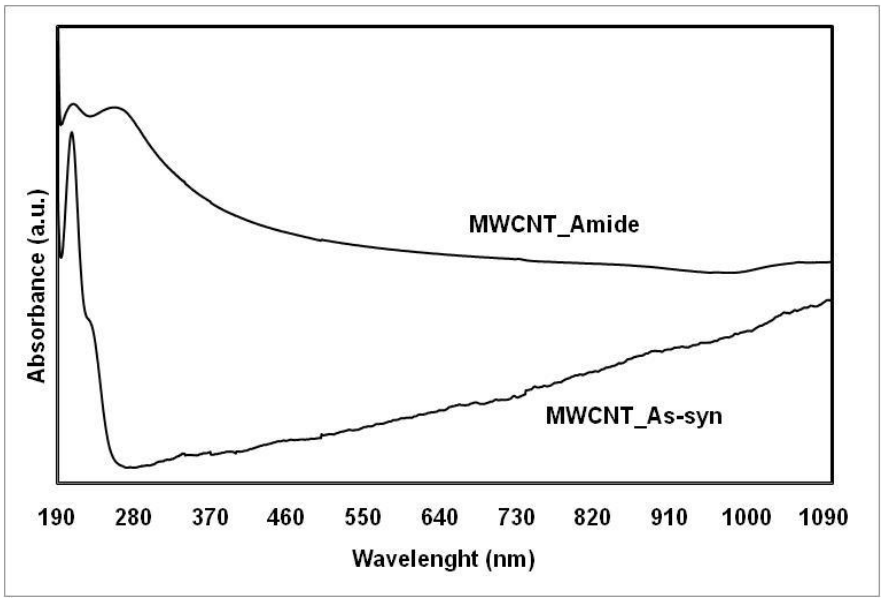

Figure B.4.4: Signals before and after the MWCNT functionalization.

The FTIR spectra of the assynthesized and functionalized MWCNT are shown in figure B.4.5. As in SWCNT-NH_2 sample, a signal due to N-H vibrations in MWCNT-NH_2 could be appreciated in the corresponding spectrum.

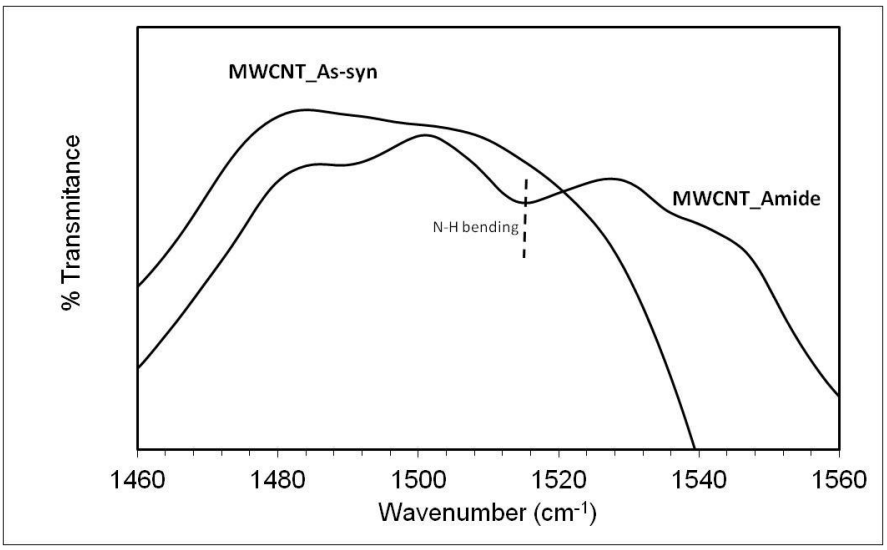

Figure B.4.5: The FTIR spectra of the assynthesized and functionalized MWCNT.

As observed with the SWCNT, before and after the functionalization procedure the Raman spectrum of the assynthesized MWCNT and MWCNT-NH_2 samples displayed in Figures B.4.6 and B.4.7 respectively, shows that the nanotubes conserved its framework, since its characteristic signals are maintained after the process.

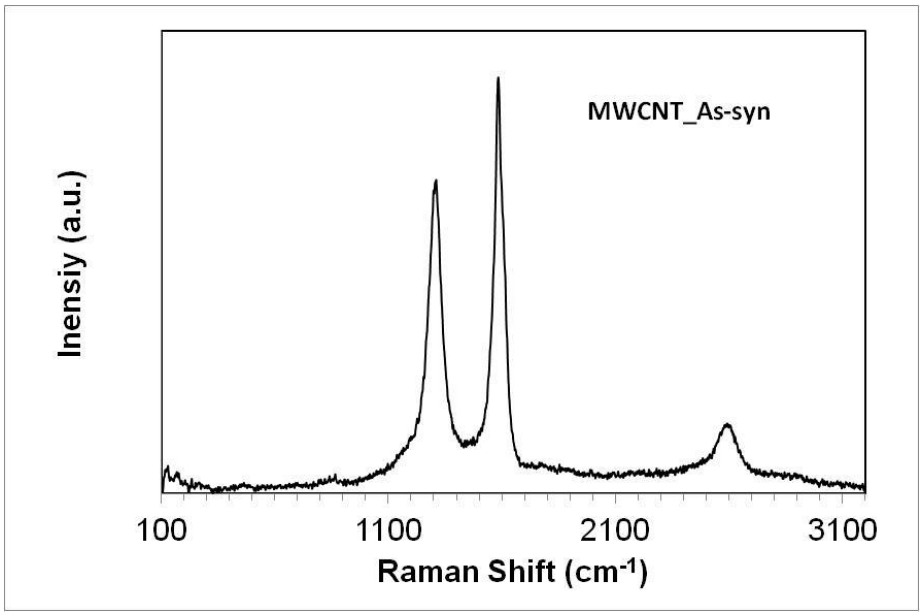

Figure B.4.6: Raman spectrum of MWCNT-Assynthesized.

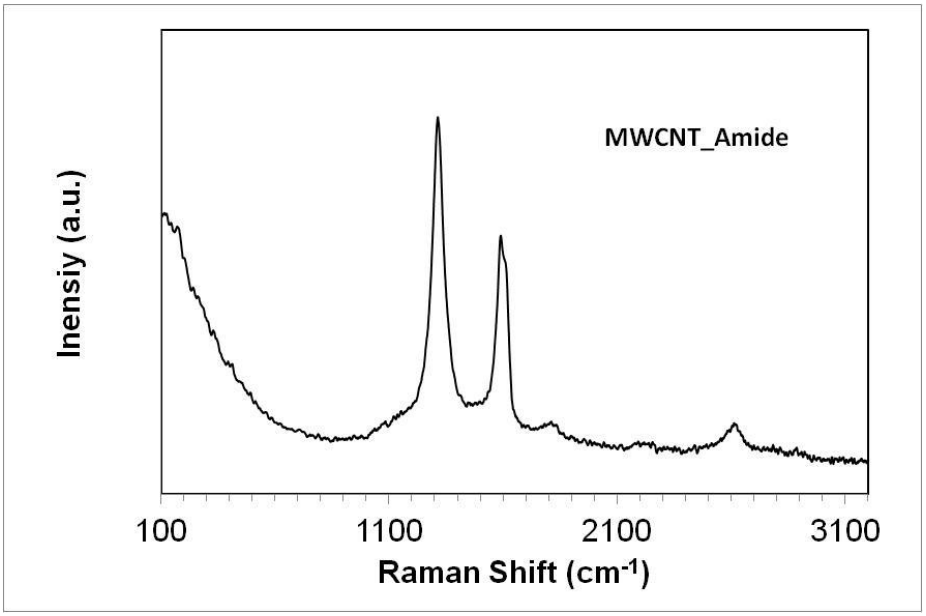

Figure B.4.7: Raman spectrum of MWCNT-NH_2.